

University of Windsor

## Scholarship at UWindor

---

Electronic Theses and Dissertations

Theses, Dissertations, and Major Papers

---

Summer 2021

# Pseudo-Zero Velocity Re-Detection Double Threshold Zero-Velocity Update Method for Inertial Sensor-Based Pedestrian

Tianyi Zhao  
*University of Windsor*

Follow this and additional works at: <https://scholar.uwindsor.ca/etd>



Part of the [Mechanical Engineering Commons](#)

---

### Recommended Citation

Zhao, Tianyi, "Pseudo-Zero Velocity Re-Detection Double Threshold Zero-Velocity Update Method for Inertial Sensor-Based Pedestrian" (2021). *Electronic Theses and Dissertations*. 8824.  
<https://scholar.uwindsor.ca/etd/8824>

This online database contains the full-text of PhD dissertations and Masters' theses of University of Windsor students from 1954 forward. These documents are made available for personal study and research purposes only, in accordance with the Canadian Copyright Act and the Creative Commons license—CC BY-NC-ND (Attribution, Non-Commercial, No Derivative Works). Under this license, works must always be attributed to the copyright holder (original author), cannot be used for any commercial purposes, and may not be altered. Any other use would require the permission of the copyright holder. Students may inquire about withdrawing their dissertation and/or thesis from this database. For additional inquiries, please contact the repository administrator via email ([scholarship@uwindsor.ca](mailto:scholarship@uwindsor.ca)) or by telephone at 519-253-3000ext. 3208.

**Pseudo-Zero Velocity Re-Detection Double Threshold Zero-Velocity Update Method for Inertial Sensor-Based Pedestrian Navigation**

by

**Tianyi Zhao**

A Thesis

Submitted to the Faculty of Graduate Studies  
through the Department of Mechanical, Automotive and Materials Engineering  
in Partial Fulfillment of the Requirements for  
the Degree of Master of Applied Science  
at the University of Windsor

Windsor, Ontario, Canada

2021

© 2021 Tianyi Zhao

**Pseudo-Zero Velocity Re-Detection Double Threshold Zero-Velocity Update Method for Inertial Sensor-Based Pedestrian**

**Navigation**

by

**Tianyi Zhao**

APPROVED BY:

---

X. Chen

Department of Electrical and Computer Engineering

---

A. Rahimi

Department of Mechanical, Automotive and Materials Engineering

---

J. Ahamed, Advisor

Department of Mechanical, Automotive and Materials Engineering

April 29, 2021

# DECLARATION OF CO-AUTHORSHIP/PREVIOUS PUBLICATION

## I. Co-Authorship

I hereby declare that this thesis incorporates material resulting from joint research as follows:

Portions of Chapters 1.1, 1.6, 1.7, Chapter 2.1 and 3.1 of this thesis were authored under the supervision of Dr. M. J. Ahamed. In this thesis, the key ideas, experimental designs, data analysis and interpretation and writing were performed by the author.

I am aware of the University of Windsor Senate’s Policy on Authorship, and I certify that I have properly acknowledged the contributions of other researchers to my thesis, and that I have obtained written permission from each of the co-author(s) to include the aforementioned material(s) in my thesis.

I certify that, with the above qualification, this thesis and the research to which it refers are the product of my own work.

## II. Previous Publication

This thesis includes [1] original papers that have been previously published/submitted for publication in peer reviewed journals, as follows:

Thesis Chapter	Publication Title/Full Citation	Publication Status*
Chapters 2-5	<i>T. Y. Zhao, M. J. Ahamed, “Pseudo-zero velocity re-detection double threshold zero-velocity update (ZUPT) for inertial sensor-based pedestrian navigation,” in IEEE Sensors Journal, doi: 10.1109/JSEN.2021.3070144.</i>	<i>Accepted (in press)</i>

I certify that I have obtained written permission from the copyright owner(s) to include the above published material(s) in my thesis. I certify that the above material describes work completed during my registration as a graduate student at the University of Windsor.

### III. General

I declare that, to the best of my knowledge, my thesis does not infringe upon anyone's copyright nor does it violate any proprietary rights, and that any ideas, techniques, quotations, or any other material from the work of other people included in my thesis, published or otherwise, are fully acknowledged in accordance with standard referencing practices. Furthermore, to the extent that I have included copyrighted material that surpasses the bounds of fair dealing within the meaning of the Canada Copyright Act, I certify that I have obtained written permission from the copyright owner(s) to include such material(s) in my thesis.

I declare that this is a true copy of my thesis, including any final revisions, as approved by my thesis committee and the Graduate Studies office, and that this thesis has not been submitted for a higher degree to any other university or institution.

## ABSTRACT

Zero-velocity update method is widely used in inertial measurement unit based pedestrian navigation systems for mitigating sensor drifting error. In the basic pedestrian dead reckoning system, especially in a foot-tie PDR system, zero-velocity update method and a Kalman filter are two core algorithms. In the basic PDR system, ZUPT usually uses a single threshold to judge the gait of pedestrians. A single threshold, however, makes ZUPT unable to accurately judge the gait of pedestrians in different road conditions. In this thesis paper, we propose a new, redesigned zero-velocity update method without using additional equipment and filter algorithms to further improve the accuracy of the correction results. The method uses a sliding detection algorithm to help re-detect the zero-velocity intervals, aiming to remove the pseudo-zero velocity interval and the pseudo-motion interval, as well as improving the performance of the ZUPT method. The method was implemented in a shoe-mounted IMU-based navigation system. For 3-6 km/h walking speed step detection tests, the accuracy of the proposed ZUPT method has an average 23.7% higher than the conventional methods. In a long-distance walking path tracking test, the mean error of the estimated path for our method is 0.61 m, which is an 81.69% reduction compared to the conventional ZUPT methods. The details of the improved ZUPT method presented in this paper not only enables the tracking technology to better track a pedestrian's step changes during walking, but also provides better calculation conditions for subsequent filter operations.

## **DEDICATION**

The greatest test of courage on earth is to bear defeat without losing heart. Fortunately, during my lonely and helpless period, many people stood by my side and gave me encouragement and support. The friends I made during the years of wandering alone are the precious wealth of my life. Especially thank to my older brother Pengzhao Song, his positive spirit has always motivated me to move forward.

To my parents, for their selfless dedication and support in helping me complete my nearly 20 years of school career. They are the people who give me life, the people who tell me how to be strong, the people who support me unconditionally. To my wife, Dewei Kong, for her understanding and encouragement. They are the most important people in my life. They will also be the ones I need to work hard to protect in the future.

Life is but a hard and tortuous journey, I will not stop.

## **ACKNOWLEDGEMENTS**

I wish to express my gratitude and thanks to my advisor, Dr. M. J. Ahamed, for his assistance and patience throughout my graduate degree, especially the help and guidance with my research topic in the past two years. I wish to thank Matthew Straeten for the technical support and for sharing the experiments' results. I would also like to thank my committee members, Dr. Afshin Rahimi and Dr. Xiang Chen, for their valuable suggestions and ideas, which helped to improve my research.

I wish to thank Natural Sciences and Engineering Research Council of Canada (NSERC) for the financial support of this research work. And I wish to thank UWindsor Research Internship for the support of this research work.



# CONTENTS

Declaration of Co-Authorship/Previous Publication .....	iii
Abstract .....	v
Dedication .....	vi
Acknowledgements .....	vii
List of Tables .....	x
List of Figures .....	xi
List of Abbreviations .....	xiv
Chapter 1: Introduction .....	1
1.1 Background .....	1
1.1.1 Pedestrian Positioning Information System .....	1
1.1.2 Outdoor Environment Positioning Technology .....	2
1.1.3 Indoor Environment Positioning Technology .....	3
1.1.4 Inertial Navigation System .....	4
1.1.5 MEMS-Based Devices .....	5
1.1.6 Pedestrian Dead Reckoning .....	7
1.2 ZUPT-Based PDR System .....	8
1.2.1 System Components .....	8
1.2.2 Zero-Velocity Update .....	11
1.3 Filtering .....	13
1.3.1 Kalman Filter .....	14
1.3.2 Gaussian Filter .....	14
1.3.3 Complementary Filter .....	14
1.3.4 High-Pass Filter and Low-Pass Filter .....	15
1.4 Existing PDR Methods .....	16
1.5 Problem Statements .....	18
1.6 Objectives and Methodologies .....	19
Chapter 2: Development of Baseline Inertial Navigation System .....	21
2.1 Physical System Design .....	21
2.1.1 IMU Sensor and Platform .....	21
2.1.2 Foot-Mounted INS device .....	23
2.2 Calibration .....	27
2.3 Data Expression .....	32
2.4 Methodology and Implementation .....	36

2.4.1 Inertial Navigation System Algorithm .....	36
2.4.2 Kalman Filter Algorithm .....	37
2.4.3 Zero-Velocity Update Algorithm .....	39
2.4.4 IMU-Based PDR Algorithm .....	42
2.5 Map Plots of Basic PDR Algorithms .....	47
2.6 Benchmark Summary.....	49
Chapter 3: Development of Pseudo-Zero Velocity Re-Detection Double Threshold	
Zero-Velocity Update Method .....	51
3.1 Conventional ZUPT Methods .....	51
3.1.1 Introduction to Two Conventional ZUPT Methods .....	51
3.1.2 Pseudo-Zero-Velocity Interval and False Detection .....	52
3.2 Pseudo-Zero-Velocity Re-Detection Double-Threshold ZUPT Method .....	55
3.2.1 Implementation Algorithm of Proposed ZUPT Method .....	55
3.2.2 The Formula Implementation Algorithm .....	60
3.2.3 New ZUPT Method's Performance and Testing Results .....	62
3.3 Low-Pass Filter .....	64
Chapter 4: Results and Discussion.....	68
4.1 Step Detection.....	68
4.2 Navigation Map Plot .....	72
4.3 Eight-Point Error Method .....	79
Chapter 5: Summary and Conclusions.....	84
5.1 Summary .....	84
5.2 Future Work .....	85
5.3 Conclusions.....	86
Reference and Bibliography .....	87
Appendices.....	93
Vita Auctoris .....	94
Appendix .....	86
Vita Auctoris .....	87

## LIST OF TABLES

Table I: MEMS Inertial Sensor Classification Comparison [8].	5
Table II: Experiment results for four PDR methods.	17
Table III: LSM9DS1 operating specifications.	22
Table IV: SparkFun LSM9DS1 Sensor Specifications.	28
Table V: Sensor Errors Determined from Allan Variance Plot.	28
Table VI: Initial Noise Variables.	31
Table VII: Data Samples Collected from IMU Sensor in CSV File.	32
Table VIII: Specific judgment of the accelerometer threshold.	41
Table IX: System initialized parameter values.	42
Table X: Device benchmark data	50
Table XI: The amount of data collected for foot phases at 3-4 km/h.	56
Table XII: The amount of data collected for foot phases at 8-10 km/h.	57
Table XIII: ZUPT Detected results from 6 s-10 s.	58
Table XIV: 60 s, 3-4 km/h Step Detection Results.	69
Table XV: 300 s, 3-4km/h Step Detection Results.	70
Table XVI: 120s, 4-6 km/h Step Detection Results.	70
Table XVII: 120s, 8-10 km/h Step Detection Results.	71
Table XVIII: The step detection results in satellite map test.	76
Table XIX: 3-4km/h long-time walking test	78
Table XX: Eight-point coordinates comparison.	81
Table XXI: Comparison between different PDR methods.	83

## LIST OF FIGURES

Figure 1. 1: Flowchart of the basic INS implementation algorithm [19].....	7
Figure 1. 2: Flowchart of the basic ZUPT-based PDR [25].....	10
Figure 1. 3: Pedestrian footsteps dynamic decomposition.....	11
Figure 1. 4: Multipath effect on direct signals.....	18
Figure 2. 1: SparkFun LSM9DS1 Breakout.....	21
Figure 2. 2: Figure 2.2: Raspberry Pi 3 Model B.....	22
Figure 2. 3: First generation of the device setup.....	24
Figure 2. 4: Second generation of the device setup.....	25
Figure 2. 5: Proposed shoe-mounted tracking device setup.....	26
Figure 2. 6: Device upgrade version for fast walking test.....	26
Figure 2. 7: Six-position static calibration method [52].....	29
Figure 2. 8: Three-position calibration method.....	30
Figure 2. 9: Acceleration data collected from 25 s walking test.....	33
Figure 2. 10: Gyroscope data collected from 25 s walking test.....	34
Figure 2. 11: The first 5 s acceleration data collected from 25 s walking test.....	34
Figure 2. 12: The first 5 s gyroscope data collected from 25 s walking test.....	35
Figure 2. 13: Flowchart of the INS phase implementation algorithm.....	36
Figure 2. 14: Stance phase and swing phase shown by the magnitude angular rate.....	40
Figure 2. 15: Estimated walking path for 25 s based on INS phase algorithm only.....	47
Figure 2. 16: Estimated walking path for 25 s based on INS phase algorithm with	

conventional single threshold ZUPT method.....	48
Figure 3. 1: Conventional method false detection of zero-velocity.....	52
Figure 3. 2: Single-threshold-with-variance method false detection of zero-velocity.....	53
Figure 3. 3: Identification of pedestrian's foot 3D walking trajectory.....	54
Figure 3. 4: Flowchart of the single-threshold ZUPT implementation algorithm [25].....	59
Figure 3. 5: Flowchart of the pseudo-zero-velocity re-detection double-threshold ZUPT implementation algorithm.....	59
Figure 3. 6: The proposed ZUPT method with no false detection.....	62
Figure 3. 7: Estimated walking path for 25 s based on the proposed ZUPT method.....	63
Figure 3. 8: Estimated walking path for 25 s based on the proposed ZUPT method with moving average filter.....	65
Figure 3. 9: Estimated walking path based on the proposed ZUPT method.....	66
Figure 3. 10: Estimated walking path based on the proposed ZUPT method with moving average filter.....	67
Figure 4. 1: Estimated walking path for 60 s based on single-threshold ZUPT method.....	72
Figure 4. 2: Estimated walking path for 60 s based on proposed ZUPT method..	73
Figure 4. 3: The 3-7 km/h walking test based on satellite map background.....	74
Figure 4. 4: 3-4 km/h long-time walking test.....	77
Figure 4. 5: Eight-point error method for single-threshold ZUPT method.....	79
Figure 4. 6: Eight-point error method for the proposed ZUPT method.....	80

Figure 4. 7: Error line graph for the conventional ZUPT method..... 82

Figure 4. 8: Error line graph for the proposed ZUPT method..... 82

## LIST OF ABBREVIATIONS

<b>CSV</b>	Comma Separated Values
<b>GNSS</b>	Global Navigation Satellite System
<b>GPS</b>	Global Positioning System
<b>HDR</b>	Heuristic Heading Reduction
<b>HMM</b>	Hidden Markov Model
<b>I2C</b>	Inter-Integrated Circuit
<b>ICs</b>	Integrated Circuits
<b>IMU</b>	Inertial Measurement Unit
<b>INS</b>	Inertial Navigation System
<b>KF</b>	Kalman Filter
<b>MEMS</b>	Micro-Electro-Mechanical Systems
<b>PDR</b>	Pedestrian Dead Reckoning
<b>SSH</b>	Secure Shell
<b>WI-FI</b>	Wireless Fidelity
<b>WSN</b>	Wireless Sensor Networks
<b>UWB</b>	Ultra-Wide Band
<b>ZUPT</b>	Zero-Velocity Update

# Chapter 1: Introduction

## 1.1 Background

### 1.1.1 Pedestrian Positioning Information System

Pedestrian positioning information system is a method for the real-time positioning of pedestrians through modern technologies [1]. Due to human beings' requirements for authenticity, convenience, and real-time information in present day society, the rapid development of this technology has been promoted. Therefore, pedestrian positioning information systems now play an increasingly important role in many applications, including assisted navigation, aiding first responders, biomedical uses, healthcare monitoring, defense, and other applications. Due to the development of personal mobile devices, the demand for location-based services is increasing, even in consumer contexts, such as cell phones, shopping malls, hospitals, and urban locations. The most popular application of pedestrian positioning information systems is seen when the Internet and personal mobile devices are used to obtain positioning information and for use in navigation, tracking, detection, information notification, and other services. Because of the extensive use of pedestrian positioning information systems, the needs for high-precision systems increases fast. The pursuit of more precise systems has always been the direction of development in this field. In consideration of the different requirements of pedestrians for information positioning in different locations, the information network developers will also choose different information network construction methods to meet the needs of different people. Moreover, the construction methods of these information networks are all based on the strength of information signals that can be collected and transmitted under different environments.

Therefore, there are two main categories for pedestrian positioning information



systems: outdoor environment positioning technology and indoor environment positioning technology.

### **1.1.2 Outdoor Environment Positioning Technology**

The main application scope of outdoor environment positioning technology is outdoor environments, which is also the most widely and frequently used positioning technology for pedestrians. Usually, to locate pedestrians' positioning information in the outdoors – and to make these outdoor technologies work accurately – the technologies need connectivity with external sources, such as routers, cell phone towers, and satellites to estimate accurate position information.

The global navigation satellite system (GNSS) [2] is widely used in outdoor environments due to its three main advantages: wide signal coverage, high positioning accuracy, and real-time position update function, which it completes by receiving and emitting satellite signals. In the satellite network coverage area, pedestrians can quickly obtain current position information through GNSS, and the error of the position information can be well controlled within a certain range. In areas with strong satellite signal coverage, the position information error can be controlled within 5-10 meters, and, in areas with weak satellite signals, the position information error can also be controlled within the interval of 20-30 meters [3], [4]. It is now the most commonly used positioning system in daily life. The GNSS is great for outdoor positioning tracking, but, for indoor positioning use, it is limited by its signals. For example, in urban environments, the tall buildings will block the satellite signals, removing the GNSS's line of sight, and will have the multipath effect, which leads to the signals being superimposed on each other to cause interference, distorting the original signal and producing errors. In some specific area, like basements, weak signal strength is another problem. The limitations of satellite signal coverage make GNSS not suitable for indoor environment positioning navigation.

### **1.1.3 Indoor Environment Positioning Technology**

As the name suggests, indoor environment positioning technology mainly focuses on indoor environments. Furthermore, this technology also performs well in some special areas that cannot be covered by satellite signals, such as suburbs, barren mountains, and forests. For humans, many activities are performed indoors, so the demand for accurate and standalone indoor positioning is becoming higher and higher. There are various approaches for indoor positioning methods. Therefore, based on these different methods, indoor environment positioning technology can be divided into two categories: infrastructure-based approaches and infrastructure-free approaches [5].

The infrastructure-based method refers to the technology for inferring indoor locations by sensing and collecting signals through pre-built indoor equipment. These pre-built devices include various communication technology facilities that are currently in wide use, such as wireless fidelity (Wi-Fi) [6], Bluetooth, wireless sensor networks (WSN), infrared, and ultra-wide band (UWB) [7]. Due to the physical limitations of indoor environments, including the area's size and temperature, as well as the cost of equipment construction, infrastructure-based methods have challenges based on their proximity and connectivity to the pre-build equipment. To overcome these, other methods are explored that do not rely on pre-built equipment.

An infrastructure-free method is one that can obtain indoor positioning data without the need to pre-arrange equipment that senses and receives signals. Because there are no constraints based on either the environment or the proximity and cost of equipment, the method without infrastructure is easier to apply and more widely popular than the method based on infrastructure. The inertial navigation system (INS) is the representative method in the infrastructure-free method.

Compared with the infrastructure-free method, the infrastructure-based method has some major shortcomings. The first major shortcoming is the area of application. Because it requires pre-built equipment when in use, and the use range of pre-built

equipment has an upper limit, this method is limited to the scope of pre-built equipment when it is used, leading to a decrease in the practicability of the device. The second major shortcoming is the cost of pre-built equipment. Because pre-built equipment is required every time the infrastructure-based method is used, the cost of pre-built equipment will be incurred every time. Compared with the infrastructure-free method, the infrastructure-based method is more expensive. After the pre-built equipment is built, this method will then face the third major problem: challenges based on the proximity and connectivity of the pre-built devices. Because the experimental site cannot be an empty site, it is a problem determining how to ensure the communication conditions of this method in the site. Therefore, considering the cost of devices and the difficulty of equipment installation, when we need to choose an indoor environment positioning method as our experimental method, the infrastructure-free method will be the first choice.

#### **1.1.4 Inertial Navigation System**

An inertial navigation system is an autonomous navigation system that does not rely on external information, such as that from a global positioning system (GPS), and does not radiate energy to the outside. Due to its own working characteristics, the INS can work in the air, on the ground, and even underwater. The basic principle of the INS is based on Newton's laws of mechanics. By measuring and collecting the acceleration of the carrier in the inertial reference system, integrating it with time, and converting it to the navigation coordinate system, the navigation coordinate system can be obtained, and the velocity, heading direction, and position information can be calculated. The advantage of the INS is that it can work in any weather, at any time, and can provide continuous navigation information with a high data update rate and good stability. Therefore, the original INS is mostly used in national armed strategy, weapon deployment, and intercontinental civil aviation flights. The cost of INS in these fields is also very expensive. With the development of micro-electro-mechanical systems (MEMS), commercial and consumer-grade inertial navigation systems can be gradually

accepted by the public. Compared with military-grade INS, the accuracy of a MEMS INS will decrease with the increase of time. Due to the influence of external factors such as noise, the drift rate generated by the movement of objects is very high. A MEMS-level INS, thus, has poor accuracy in long-term use. Therefore, when using a civilian-level INS, a complete calibration mechanism and filter algorithm are required to ensure the accuracy of the navigation system. Table I shows the comparison between different classifications of MEMS inertial sensors [8].

<b>TABLE I</b>			
<b>Application Scenario</b>	<b>Bias Stability level</b>	<b>System Price Range</b>	<b>Control Level</b>
Consumer electronics	Low	Under one hundred dollars	High
Car ESP and navigation system	Medium	Thousands of dollars	Medium
Military and aerospace grade	Medium	Millions of dollars	Low

**Table I: MEMS Inertial Sensor Classification Comparison [8].**

### **1.1.5 MEMS-Based Devices**

A micro-electro-mechanical system sensor is a combination of electronic and mechanical hardware in chip form. Each MEMS sensor is composed of micro-silicon structures, and these silicon structures are embedded into the silicon wafer through a special etching process. These kinds of inertial sensors are microscale devices ( $10^{-6}$  m) that utilize both mechanical and electrical systems to provide sensing ability. In recent years, through continuous improvement of sensors, including their cost, size, and accuracy, MEMS-based inertial sensors can be used in multiple applications of personal electronic platforms, especially wearable smart device platforms.

MEMS-based inertial sensors work through the employment of a mass, which is driven to resonance by an electrical circuit. Taking a gyroscope as an example, the resonance mass of the gyroscope will be displaced by the action of the Coriolis force, and then the change in capacitance caused by the change in the distance between the electrodes is measured to sense the angular velocity. Within this work, two types of inertial sensors will be utilized, a gyroscope and an accelerometer. An accelerometer is a sensor that senses axial acceleration and converts it into a usable output signal; a gyroscope is a sensor that can sense the angular velocity of a moving body relative to inertial space. Three MEMS accelerometers and three MEMS gyroscopes are combined to form an inertial measurement unit [9], [10], [11] that can sense the angular velocity and acceleration of the carrier in three directions.

Different from traditional inertial devices, because of the development of MEMS, today's IMU is no longer limited to the use of professional navigation, as in military navigation. MEMS technology helps IMU improve the shortcomings of traditional inertial devices, such as their high prices, large volumes, small precision adjustment ranges, and single application fields [12], [13]. As a result, IMU has entered the field of low-priced electronic consumer products. The characteristics of this type of MEMS-based IMU are low unit prices, small sizes, and narrow temperature ranges. These features help IMUs expand the application field, especially in the development of personal devices – for example, the pedestrian dead reckoning (PDR). MEMS-based IMU has two kinds of inertial sensors, and is characterized by its small size and wearability, which is exactly what PDR technology needs. In addition, the low unit price feature means the IMU can be widely used in PDR systems, and it can be easily accepted by the public [14].

### 1.1.6 Pedestrian Dead Reckoning

Inertial navigation system (INS) is the widely used system in the infrastructure-free field. Figure 1.1 shows the flowchart of the basic inertial navigation system's implementation algorithm. In the INS system, the representative method is PDR [15], [16]. PDR is a technique that uses the inertial measurement unit to estimate the position of the pedestrian. The principle of PDR is to calculate the pedestrian's walking trajectory, position, and other information by measuring and counting the number of steps, step length, and direction of the pedestrian [17], [18].

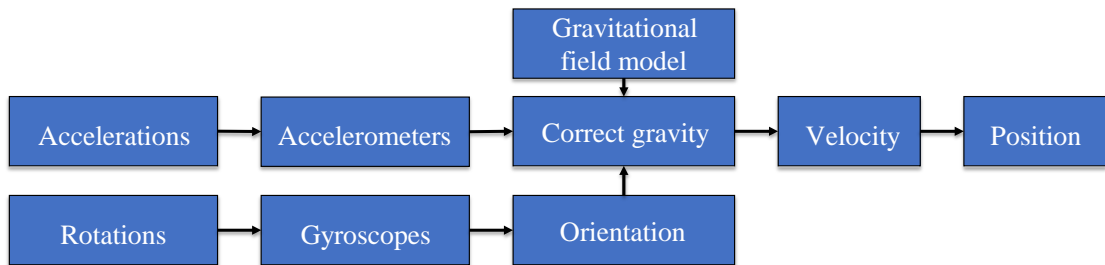


Figure 1. 1: Flowchart of the basic INS implementation algorithm [19].

The traditional PDR system uses the data collected by the IMU to perform integral calculations to obtain the walking trajectory of pedestrians [19]. The PDR system collects data by operating two inertial sensors of the IMU while the pedestrian is walking. The accelerometer collects the acceleration values corresponding to the three axes of X, Y, and Z at each moment, and the gyroscope collects the corresponding angular velocity on the same three axes at the same time. Acceleration is calculated through integration to obtain speed and displacement, and angular velocity is calculated to obtain changes in the direction of pedestrian walking. The pedestrian walking path information can be estimated by combining the two resulting values. Integral operation has certain requirements for the accuracy of the collected data because the low-cost, consumer-grade IMU device will be affected by noise when moving, resulting in data drift [20]. This will cause uncontrollable displacement errors and attitude errors in PDR systems based on integral operations. Therefore, to improve the accuracy of the PDR system, it is necessary to perform algorithmic error removal processing on the system.

By adding filters to filter out the errors that may occur during the IMU working process and then assisting with the zero-velocity update (ZUPT) algorithm, it can help the basic PDR system in performing path simulation. In the pedestrian walking process, the IMU sensor continuously collects data value, even if the pedestrian is in a static state. Each group of data will be integrated by the PDR system to calculate the displacement. If it is impossible to judge the walking state of the pedestrian – moving or stationary – the data in the stationary state calculated by the integral will be added to the pedestrian walking path as valid displacement data, which will cause our final estimated path to contain a large drifting error. The addition of the ZUPT method allows us to judge the walking state of pedestrians and classify them, so that the PDR system only integrates the data in the motion state, controlling the displacement errors. Therefore, the ZUPT method is an indispensable part of the basic PDR system algorithm. Next, the structure and working principle of the ZUPT method-based PDR system will be introduced, and the data will be studied for the gait of pedestrians, and how to determine the zero velocity interval through the gait changes will be discussed.

## **1.2 ZUPT-Based PDR System**

### **1.2.1 System Components**

The most basic PDR principle is to obtain acceleration and angular velocity data from the IMU sensor and process the acquired data through algorithmic calculations to obtain pedestrian's walking path. Because of the accumulation of errors generated by the sensor during work, the inaccuracy of the integral calculation is increased. Therefore, when the PDR system is designed, data constraints around the basic principles are used to obtain a more accurate trajectory. Kalman filter and zero-velocity update method [21], [22], [23], [24] are often used for data processing and error control.

The working algorithm for the ZUPT-based PDR system can be formulated

summarized as [25]:

1. Accelerometers and gyroscopes provide information about axial accelerations and angular velocity.
2. The gravity vector is removed from acceleration information.
3. Gyroscope values are integrated to provide rotational displacement since the last sample.
4. The orientation in the navigation frame is determined.
5. Accelerations are transformed from inertial frame to navigation frame, then integrated for velocity, then integrated again for displacement.
6. Kalman filter is used to estimate error covariance [26].
7. Zero-velocity update method is used to detect walking gait phases and correct errors.

Therefore, according to the above process, the ZUPT-based PDR system can be divided into three phases: INS, KF prediction, and ZUPT. Figure 1.2 shows the flowchart of the basic ZUPT-based PDR system implementation algorithm. The INS phase is responsible for orientation estimation and position calculation, the KF prediction phase is responsible for estimating the error covariance, and ZUPT is responsible for judging the swing and stance phases of pedestrians and correcting the errors generated during the walking process. This research focuses on how to optimize and improve the accuracy of the ZUPT method in the PDR system. To improve the accuracy of the ZUPT method, we need to analyze its working principle.



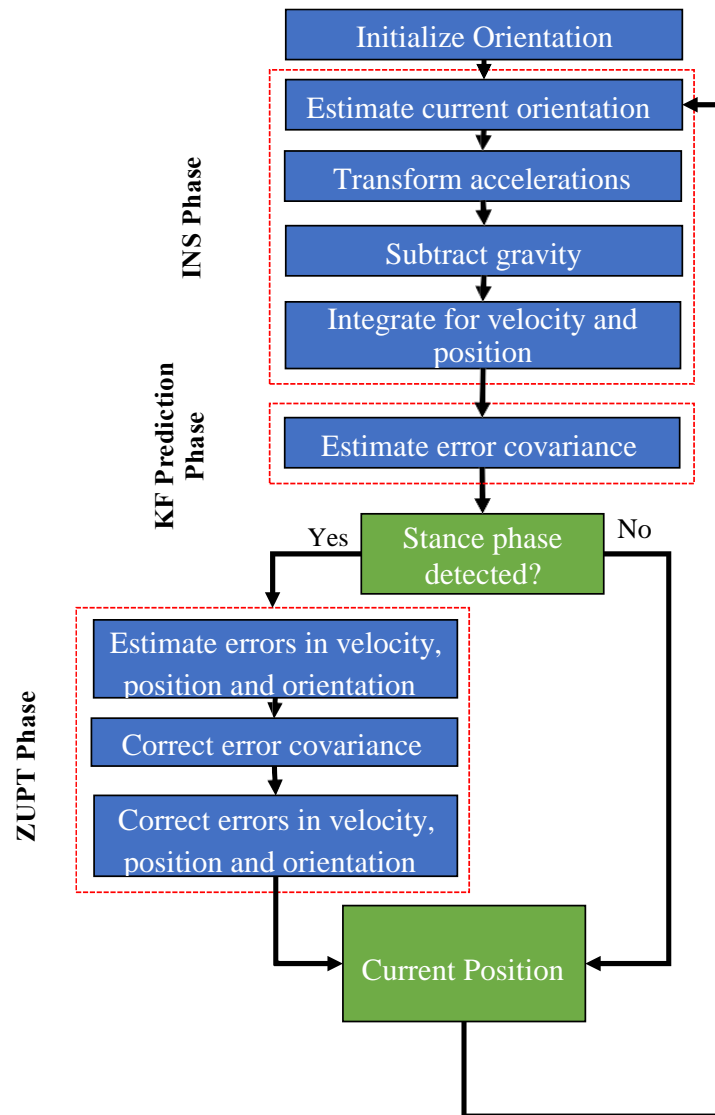


Figure 1. 2: Flowchart of the basic ZUPT-based PDR [25].

### 1.2.2 Zero-Velocity Update

The zero-velocity update method (ZUPT) is widely used to mitigate the drift error accumulated by MEMS inertial sensors in long-distance navigation [27], [28].

The principle of ZUPT is to analyze the pedestrian's gait based on the movement characteristics of their footsteps during walking; this is done to estimate step length during the movement process and to correct errors during the process of being stationary. As shown in Figure 1.3, the footsteps' movements of the pedestrian walking can be divided into two phases: swing phase and stance phase. Therefore, ensuring that the ZUPT correctly distinguishes between swing phase and stance phase is the key to eliminating drift error to a greater extent. The stance phase is the period from when the heel touches the ground until the forefoot leaves the ground, while the swing phase is

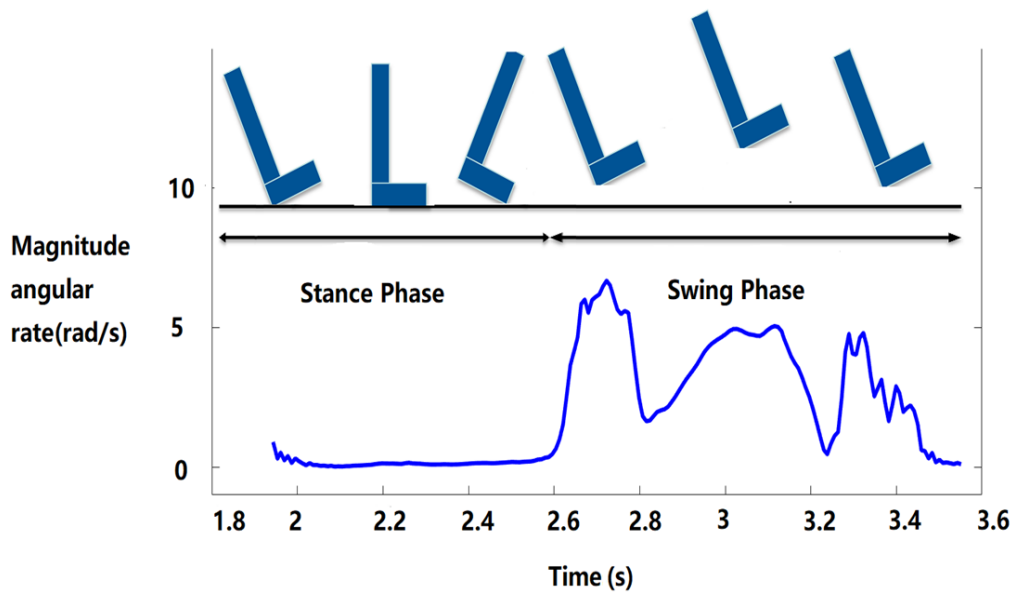


Figure 1. 3: Pedestrian footsteps dynamic decomposition

when the feet are completely suspended in air [29]. Therefore, ZUPT can help to identify the walking motion of pedestrians, tracking the number of pedestrian steps by performing dynamic judgment on the data output from IMU devices, which better completes the positioning estimation.

At present, ZUPT has been developed in many versions, and it differs under different navigation algorithms [30], [31], [32], [33], [34]. In the basic pedestrian dead reckoning (PDR) system – especially in the foot-tie PDR system – zero-velocity update method and Kalman filter are two core algorithms. In the basic PDR system, ZUPT usually uses a single threshold to judge the gait of pedestrians. In reality, however, the limitation of a single threshold makes ZUPT unable to accurately judge the gait of pedestrians in different road conditions. From this, the double-threshold ZUPT method is derived. The double-threshold ZUPT largely solves the problem of gait detection when pedestrians are walking, but the lack of stability in long-distance range walking tests due to the two fixed thresholds means that the drifting errors cannot be removed perfectly. Therefore, the current research trend of PDR for the double-threshold ZUPT method is adding other filter algorithms besides the Kalman filter to help PDR reduce the displacement error during walking. The variance method is one of them [34]. The variance method is based on the double-threshold ZUPT method. After detecting a set of walking data with two fixed thresholds, the PDR system calculates the variance in data. If the range of variance is outside the pre-set range, it means that an error has occurred, and the error data will be compensated. The variance method makes up for the shortcomings of the narrow applicability of the fixed threshold, causing the data to have better stability. Due to the functional limitation of the low-cost IMU, however, the large amount of calculations involved in the variance method makes this algorithm only suitable for short-distance walking tests. In long-distance range tests, the output results of this method are delayed.

When ZUPT can help PDR perform pedestrian gait analysis, we need some media to help ZUPT apply the judgment results to the PDR system. The filters, such as the

Kalman filter, can very well help ZUPT to do this work. These filters will help ZUPT transfer the judged data to the INS phase of the PDR system, filter the final output, and improve the PDR system's estimation results of pedestrian walking paths.

### **1.3 Filtering**

Filtering is the operation of remove specific band frequencies in the signal, and it is an important measure to suppress and prevent interference. It is a probabilistic method to estimate a related random process based on the result of observing a certain random process.

Filtering is an important concept in signal processing. There are two types of filtering: classical [35], [36], [37]and modern [38]. Classic filtering is an engineering concept based on Fourier analysis and transformation. According to advanced mathematics, any signal that satisfies certain conditions can be regarded as a superposition of infinite sine waves. Modern filtering uses analog electronic circuits to filter analog signals. The basic principle is to use the frequency characteristics of the circuit to select frequency components in the signal. According to frequency filtering, the signal is regarded as an analog signal superimposed by sine waves of different frequencies, and the signal filtering is realized by selecting different frequency components.

In inertial navigation systems, filters are widely used to help eliminate the noise in the desired signal collected by the IMU; this is done to reduce the influence of errors caused by noise. Next, the working principles of some commonly used INS filters will be introduced. In subsequent chapters, the algorithm of each filter will be introduced in more detail.

### **1.3.1 Kalman Filter**

A Kalman filter is a recursive linear filtering method developed by Rudolf Emil Kalman in 1960 [39]. A Kalman filter uses the system input and output observation data to optimally estimate the system state. Since the observation data includes the influence of noise and interference in the system, the optimal estimation can also be regarded as a filtering process. A Kalman filter can estimate the dynamic state of a series of data with measurement noise when the measurement variance is known.

It has two characteristics: (1) it can update and process the data collected on site in real time, and (2) it is very convenient to program with a computer. Therefore, Kalman filters are currently the most widely used filtering method, with very good development prospects, and are widely used in many modern engineering fields, such as communications, navigation, guidance, and control [40].

### **1.3.2 Gaussian Filter**

The Gaussian filter is a linear smoothing filter mainly used to eliminate Gaussian noise. It is widely used in the noise reduction process of image processing [41]. Gaussian filtering smoothes the edges of the image and eliminates noise by performing weighted average processing on the image.

In the inertial navigation system, the Gaussian filter is a mathematical filter. It establishes a mathematical model, transforming image data according to this model. The converted image data has high and low frequency parts, and the high frequency part belongs to noise. The Gaussian filter smoothes this part of the high-frequency data, thereby improving the accuracy of the pedestrian's final path simulation map.

### **1.3.3 Complementary Filter**

The complementary filter is a simple filter. It takes a weighted average of two or more signals, combining the weighted data to generate the required value estimate. The

complementary filter is generally comprised of a high-pass filter and a low-pass filter. The data with high-frequency noise will pass through the high-pass filter, and the data with low-frequency noise will pass through the low-pass filter, and the two pieces of data will be weighted, making the sum of the weights equal to 1. These complementary measurements produce a full measure of the desired information. INS often uses complementary filters for data processing, which is mainly used to calculate the direction. Compared with KF, however, the advantage of the complementary filter is very small. The advantage is that, if the noise of the sensor is random and obeys a normal distribution, the complementary filter can better perform error correction without making too many assumptions about the error model [42].

#### **1.3.4 High-Pass Filter and Low-Pass Filter**

A high-pass filter is a filter that allows frequencies higher than a certain cutoff frequency to pass and attenuates low-frequency signals. For a piece of signal data, if there is signal interference in the low frequency, a high-pass filter is needed to process the signal data to remove the error signal in the low frequency and to improve the accuracy of the signal. The principle of the low-pass filter is like the high-pass filter, except that the intercepted frequency signal is different [43], [44].

In an inertial navigation system, the sensor will produce errors due to noise during operation. The high-frequency characteristics of the noise will affect the subsequent data processing of the inertial navigation system, while, at the same time, reducing the accuracy of short-period inertial components. Therefore, based on the high-frequency characteristics of noise, the inertial navigation system will use a low-pass filter to reduce the noise of the high-frequency signal, eliminate the high-frequency signal of the original data, and improve the position measurement accuracy of the inertial navigation. In subsequent chapters, this thesis will also give a detailed introduction on how to build a low-pass filter model.

## 1.4 Existing PDR Methods

Due to the development of MEMS technology, the design of IMU has also become diversified. In the field of practical application, inertial navigation benefits from the diversification of IMU design, and various inertial navigation methods and algorithms are also derived.

In the field of PDR navigation, the current inertial sensor-based PDR methods can be divided into three types: foot-wear method [45], [46], leg-wear method [47], and waist-wear method [48], [49]. In addition, the path estimation algorithm in these PDR methods is different. Because pedestrians wear the sensors at different positions and the sensors experience different inertias during the walking phase, different algorithm need to be used to analyze and calculate the data when estimating the path.

Previously, there have been four PDR algorithms based on different wearing methods that have achieved relatively good results in path estimation. Table II below shows the results of experiments with these four methods.

Among these methods, the quaternion vector-based PDR method is based on a smartphone's built-in IMU sensor [50]. It is a handheld device that uses the quaternion principle to estimate the attitude. One challenge in this method is that it has a Euler integration singularity problem. Another method is the waist-mounted PDR system, which is based on an IMU sensor; the device is worn on the waist [48]. This method uses the heuristic heading reduction algorithm (HDR) and a hidden Markov model (HMM) [51] to combine Kalman filter and zero-velocity update method to track pedestrian position. The dual-mounted IMU PDR method is based on an IMU sensor, without using GPS [47]. It uses dual-mounted sensors, which were worn on legs and feet. The purpose of using two IMUs is to establish a joint constraint between the IMUs and to decrease the heel strike impact. Due to the restraint between the two IMUs, this method does not require an additional filter algorithm for error mitigation. Additional sensors are also used in PDR-based navigation – for example, an ultrasonic sensor-

integrated PDR method, which is also based on an IMU sensor combined with ultrasonic sensor for error correction. This is a foot-mounted sensor method, combined with the ultrasonic sensor module. It uses the Kalman filter and zero-velocity update method to help estimate the walking path [24], [25].

The four PDR methods introduced above produce different results due to different wearing methods, algorithms, and error mitigation approaches. Some require additional sensors or algorithms to obtain better path tracking results. Due to the use of additional sensors and algorithms, however, the overall PDR system often becomes complex; therefore, simple solutions are sought.

<b>TABLE II</b>			
<b>Method</b>	<b>Experiment</b>	<b>Error</b>	<b>Percentage</b>
Quaternion vector-based PDR	380 m walking route	2.57 m	0.68%
Waist-mounted PDR	64.48 m walking route	1.934 m	2.99%
Dual-mounted PDR (foot- and leg-mounted)	23 m walking route	0.286 m	1.24%
Ultrasonic sensor foot-mounted PDR	120 m walking route	0.53 m	0.44%

**Table II: Experiment results for four PDR methods.**



## 1.5 Problem Statements

In the current market, GNSS is already a very mature technology, with very accurate positioning technology in outdoor environments. It is able to provide long-term and stable location tracking services. Moreover, as the coverage of today's signal networks and signal strength have increased, especially with the popularization of 5G signal networks, signal services have reached a new level, with the rapid development of GNSS technology. It cannot be ignored, however, that the scope of human activities is not limited to the outdoors. In more indoor activities, GNSS is often incapable. For example, in urban settings, tall buildings will block the satellite signal, making the GNSS lack a line of sight and will have the multipath effect [52], which leads to the signals superimposed on each other to cause interference, distorting the original signal

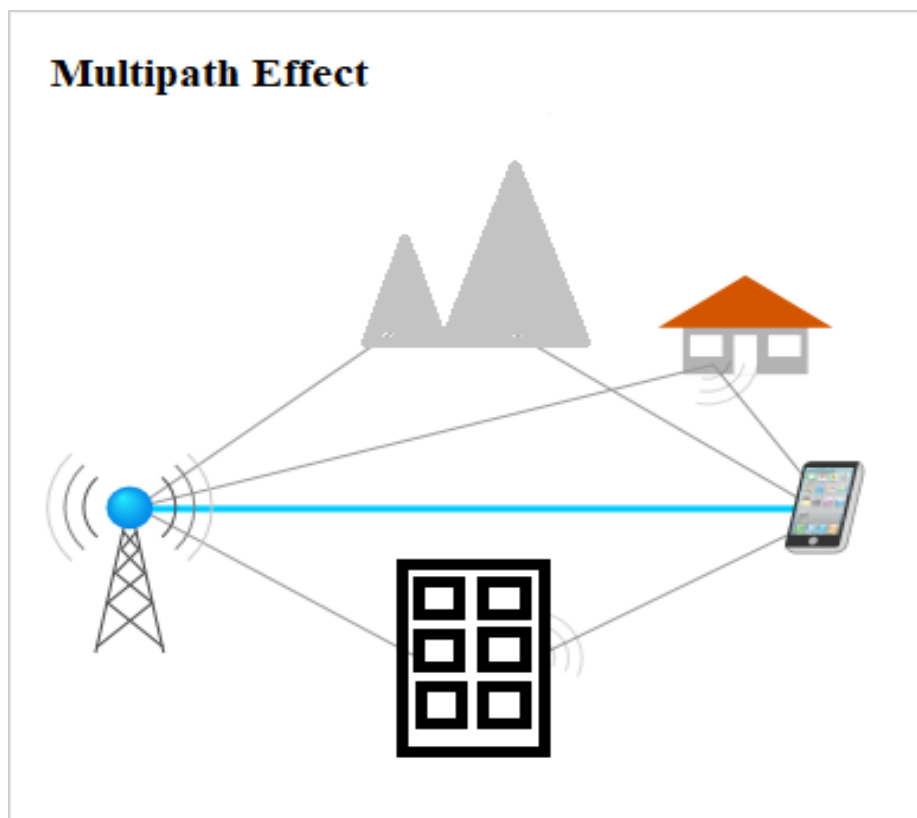


Figure 1. 4: Multipath effect on direct signals.

and producing errors. Figure 1.4 shows that the multipath effect happens on the direct signals due to the scatterers like buildings and mountains. In some specific area, like basements, poor signal strength is another problem. The limitations of satellite signal

coverage make GNSS not suitable for indoor positioning navigation.

Accurate indoor navigation yields strong potential for visually impaired persons, military and emergency service applications, and virtual reality. The shortcomings in inertial navigation, however, still need to be solved: the high cost of accurate sensing capabilities and the external navigation aids that are difficult, costly, and time consuming to implement. For the disadvantages in the existing PDR system, there are high computational requirements for standalone devices in implementing complex error correction algorithms. So, additional equipment is required for error correction. The PDR system does not only use one sensor to help track the pedestrian position, which means the integration of multiple devices increases the difficulty and cost of PDR system design. All these systems have uneven accuracy.

Therefore, for the development of PDR, it has always been crucial to:

1. Improve the stability of the system,
2. Improve the accuracy of positioning calculations,
3. Simplify the complexity of the PDR system,
4. Reduce costs.

To solve the current problems of the PDR system, research goals and methods are proposed based on these problems.

## **1.6 Objectives and Methodologies**

Within this thesis, system augmentations will be investigated to reduce navigation system errors, especially to improve the accuracy of the ZUPT method without the use of bulky or computationally expensive sensors.

Firstly, an investigation into conventional foot-mounted PDR system with ZUPT

method will be described, discussing its strengths and shortcomings in the navigation field and the caveats experienced in its implementation such as physical system design and setup, IMU sensor calibration and filters using.

Next, analyzing the data results of the conventional PDR system, summarizing the walking habits of pedestrians, and proposing a new ZUPT method to improve the positional accuracy. Without adding additional sensors, by performing secondary detection and correction on the pseudo zero velocity intervals generated during data processing, the accuracy of step detection is improved, and the purpose of controlling drift errors is achieved.

Finally, the proposed ZUPT method will be validated through several experiments, showing improvements that have been made over the conventional ZUPT methods, proving that the proposed ZUPT method has the ability to improve the zero velocity detection results. The walking path estimation experiments prove that the proposed ZUPT method can help the basic PDR system have more accuracy positioning results.

# Chapter 2: Development of Baseline Inertial Navigation System

## 2.1 Physical System Design

### 2.1.1 IMU Sensor and Platform

The IMU sensor used in this thesis is SparkFun LSM9DS1 Breakout. It is a versatile, motion-sensing system-in-a-chip. Additionally, it is a system-in-package featuring a 3D digital linear acceleration sensor, a 3D digital gyroscope sensor, and a 3D digital magnetic sensor. LSM9DS1 has a total of 9 degrees of freedom on its single board. The LSM9DS1 includes an I2C serial bus interface supporting standard and fast mode (100 kHz and 400 kHz) as well as an SPI serial standard interface. The LSM9DS1 is one of only a handful of ICs that can measure three key properties of movement – angular velocity, acceleration, and heading – in a single IC. Through these three properties, LSM9DS1 can measure the motion information of objects in three dimensions, generating nine pieces of data corresponding to acceleration, angular

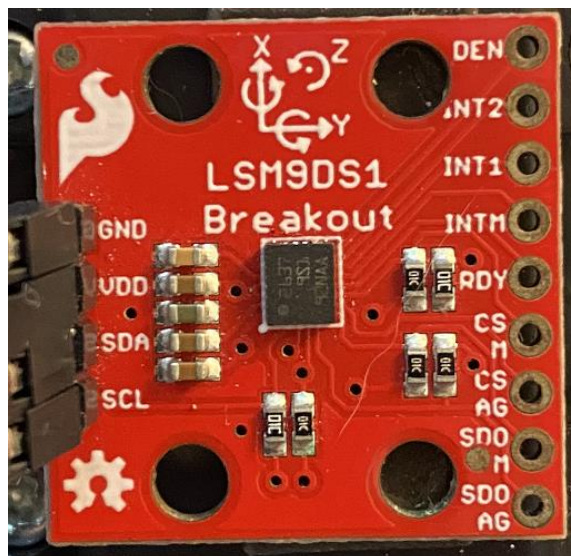


Figure 2. 1: SparkFun LSM9DS1 Breakout.

velocity, and magnetic data. Figure 2.1 shows the picture of SparkFun LSM9DS1 breakout. Table III shows the operating specifications of LSM9DS1.

TABLE III	
LSM9DS1 Specifications	Values
Operating Voltage	3.3 V
Operating Temperature Range	-40 °C to +85 °C
Full Scale for the Accelerometer	$\pm 2g/\pm 4g/\pm 8/\pm 16 g$
Full Scale for the Gyroscope	$\pm 245/\pm 500/\pm 2000 dps$
Full Scale for the Magnetic Field	$\pm 4/\pm 8/\pm 12/\pm 16 gauss$

**Table III: LSM9DS1 operating specifications.**

To control the IMU sensor, the Raspberry Pi is used as the platform for LSM9DS1. Raspberry Pi is a series of small, single-board computers. The model used is Raspberry

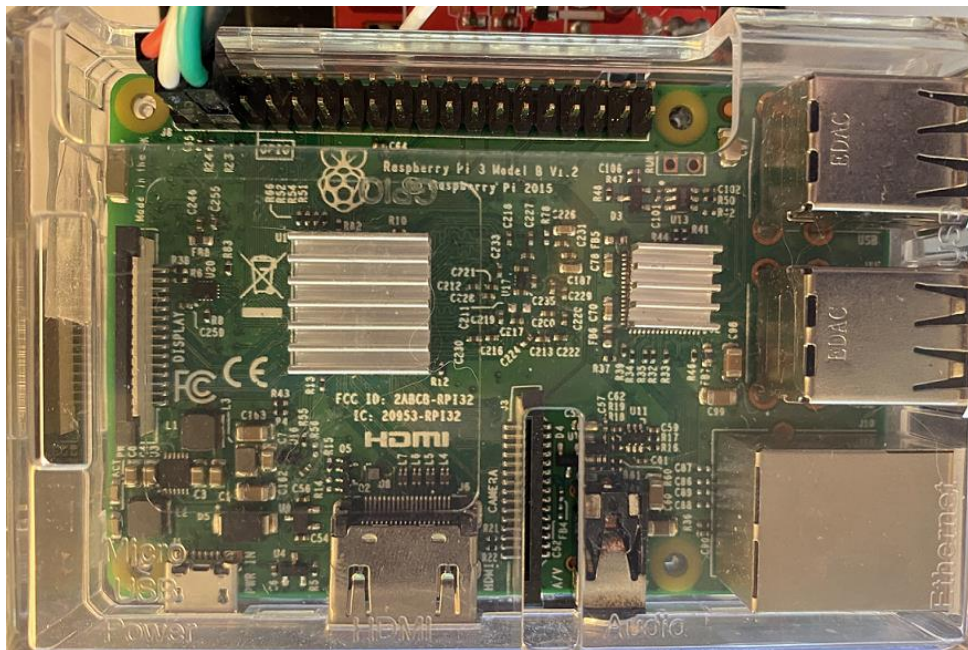


**Figure 2. 2: Figure 2.2: Raspberry Pi 3 Model B.**

Pi 3 Model B. Figure 2.2 shows the picture of raspberry pi 3 which used in this thesis. It has 1.2 GHZ 64-bit quad core ARM Cortex-A53 processor, on board 802.11n Wi-Fi, Bluetooth, and USB boot capabilities. It helps control the LSM9DS1 with the Python programming code through SSH client PuTTY software.

Through the IMU sensor and Raspberry Pi platform, we can build a PDR device system. Because LSM9DS1 has the characteristics of being small in size and wearable, we can mount the IMU sensor on the parts of the pedestrian's body, such as arms, waist, and feet. Then we can control LSM9DS1 through the Raspberry Pi platform, collect accelerometer and gyroscope data, and store them in CSV format files. The saved inertial data will be used for subsequent pedestrian path estimation.

After determining the specifications of the sensor and the operating platform, we need to design a stable structure that can mount the device to facilitate us collecting data on the sensor when pedestrians are walking.

### **2.1.2 Foot-Mounted INS device**

Because it is necessary to obtain and calculate the data of pedestrian displacement through the swing of the pedestrian's footsteps, the INS device needs to be designed as a wearable foot-mounted device. The design requirements of the device are: (1) Raspberry pi and IMU can be placed; (2) the IMU can maintain stability during the pedestrian's movement; and (3) the coordinate axis direction of the IMU should be consistent with the direction of the foot.

Figure 2.3 shows the first generation of this thesis device setup. In this device setup, the IMU sensor was putted in a bag which was mounted on the ankle. Because this method is mounted near the ankle, it cannot fully detect the movement characteristics of the footsteps, and because the bag where the IMU sensor is placed is not stable enough, it will produce additional vertical sliding errors, so this method is abandoned. The experience summarized from the first-generation device setup is: (1)

The IMU sensor needs to collect complete data consistent with the movement of the foot; (2) During the walking test, it is necessary to provide a more stable working environment for the IMU sensor.



**Figure 2. 3: First generation of the device setup.**

Figure 2.4 shows the upgrade result of the first-generation device setup. In this device setup, the IMU sensor was pasted on the front top of the shoe. In this upgrade, the data collected by the IMU sensor can be the same as the foot movement, and the device also has a certain degree of stability in short-distance walking experiments. However, due to the instability of the fixing method of the IMU sensor, the IMU sensor may slip and fall during long-distance walking experiments. Therefore, the IMU sensor needs a structure that can have stronger stability while ensuring consistency with the

foot movement.



**Figure 2. 4: Second generation of the device setup.**

Figure 2.5 shows the structure designed for the INS device. The IMU sensor and Raspberry Pi 3 are fixed to the side of the shoe with a Z-shaped aluminum alloy support plate. The bottom end of the Z-shaped bracket is inserted into the sole to ensure that unnecessary shaking will not occur when walking. This structure provides the INS device with a motion state that is the same as that of the foot so that the IMU sensor can unrestrictedly obtain the pedestrian's acceleration and the angle of foot rotation when the pedestrian is walking.

As the variety of experiments increases, such as multi-speed, long-distance testing, the shortcomings of the device structure have also been revealed. In the running test, due to the fixed method of the Z-shape structure, a vibration error was generated in the fast-walking speed test. To reduce these vibration errors, a new structure was designed shown in Figure 2.6. Figure 2.6 shows that the Z-shape frame was nailed in the shoe's



sole, which can provide a more stable working environment for the IMU sensor during more strenuous exercise.

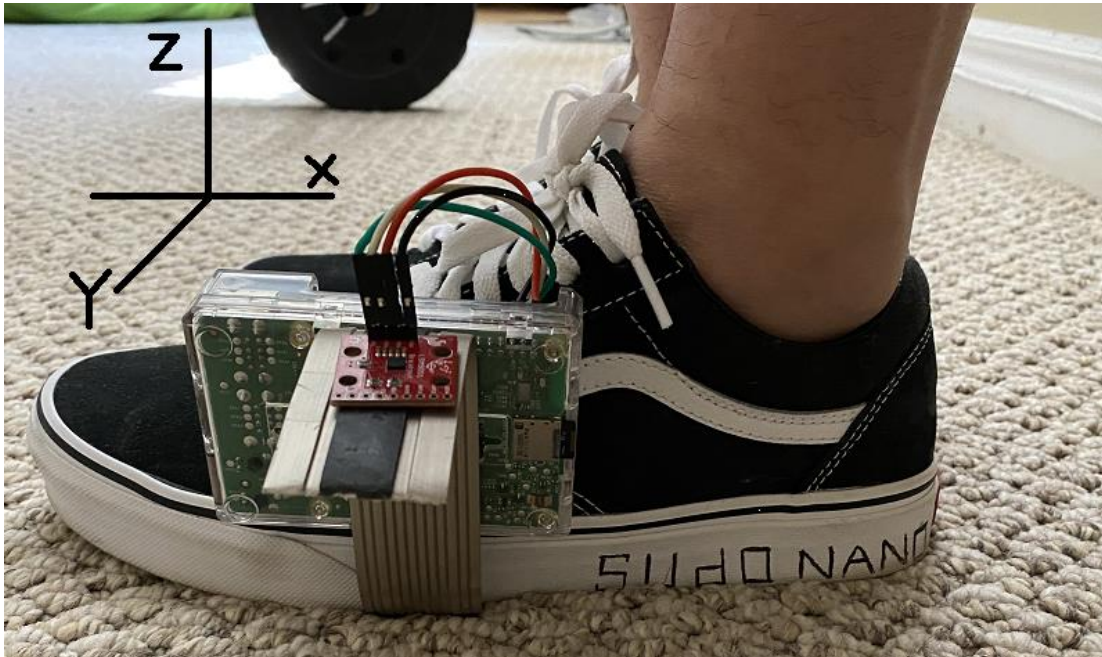


Figure 2. 5: Proposed shoe-mounted tracking device setup.



Figure 2. 6: Device upgrade version for fast walking test.

Since then, the device setup can adapt to walking tests at various speeds and can

provide a stable working environment for the IMU sensor, and the structure can also enable the IMU sensor to collect data consistent with the movement of the foot, and better help the PDR to estimate the positioning information.

After completing the design of the device structure, it is necessary to perform the corresponding calibration according to the placement of the IMU sensor to ensure that the IMU sensor will not be interfered by the bias during the working process. Calibration is also an important part of the preliminary preparations. It can help the IMU sensor to achieve the best working condition and minimize the impact of errors caused by bias.

## **2.2 Calibration**

After fixing the IMU sensor and platform, the IMU for the calibration step needs to be prepared. Before all tests are performed, the gyroscope and accelerometer of the IMU need to be calibrated to ensure that the IMU can provide maximum accuracy during operation.

In the first step, the sensor error needs to be calculated according to the output characteristics of the IMU sensor, especially the bias instability for each axis of the sensor. This bias value can allow us to understand the motion characteristics of the IMU more clearly during work, which is convenient for subsequent data processing and reduces the occurrence of errors. From the LSM9DS1 IMU device datasheets, the relevant sensor specifications are listed in Table IV. According to the information provided in the table, the data can be further quantified through the Allan variance method to obtain the required error interval and value. Allan variance is a method developed by David Allan which measures the frequency stability of oscillators and is commonly used in measuring the stability of MEMS devices [53]. Table V [25] shows the relative bias instability change value of the LSM9DS1 sensor obtained by the Allan variance method, which needs to be used in the path tracking tests.

TABLE IV			
Parameter	Setting	Typical Value	Unit
Acceleration Sensitivity	$\pm 2$ g	0.061	mg/LSB
Acceleration Sensitivity	$\pm 4$ g	0.122	mg/LSB
Acceleration Sensitivity	$\pm 6$ g	0.183	mg/LSB
Acceleration Sensitivity	$\pm 8$ g	0.244	mg/LSB
Acceleration Sensitivity	$\pm 16$ g	0.732	mg/LSB
Angular Rate Sensitivity	$\pm 245$	8.75	mdps/digit
Angular Rate Sensitivity	$\pm 500$	17.50	mdps/digit
Angular Rate Sensitivity	$\pm 2000$	70	mdps/digit
Angular Rate Zero-Rate	$\pm 245$	$\pm 10$	dps
Angular Rate Zero-Rate	$\pm 500$	$\pm 15$	dps
Angular Rate Zero-Rate	$\pm 2000$	$\pm 25$	dps

Table IV: SparkFun LSM9DS1 Sensor Specifications.

TABLE V					
Sensor Type	Axis	Angle (Velocity) Random Walk	Unit	Bias Instability	Unit
Accelerometer	X	0.001292	m/s/h <sup>0.5</sup>	0.000632	m/s <sup>2</sup>
	Y	0.001201	m/s/h <sup>0.5</sup>	0.000585	m/s <sup>2</sup>
	Z	0.001242	m/s/h <sup>0.5</sup>	0.000504	m/s <sup>2</sup>
Gyroscope	X	0.000143	rad/h <sup>0.5</sup>	0.000214	rad/s
	Y	0.012323	rad/h <sup>0.5</sup>	0.000321	rad/s
	Z	0.000297	rad/h <sup>0.5</sup>	0.000297	rad/s

Table V: Sensor Errors Determined from Allan Variance Plot.

Since the IMU will produce the above-mentioned bias on the accelerometer and gyroscope, after being used for a period, it is necessary to calibrate the IMU before each experiment. In the second step, the accelerometer and gyroscope of the IMU sensor need to be calibrated. The calibration method comes from the RTIMULib IMU programming file of Github [54]. This file provides calibration procedures for the accelerometer and gyroscope, respectively. For the accuracy calibration of the accelerometer, the program uses the six-position static calibration method. The principle of this method is to compare the accelerometer data collected in six different coordinate directions with the factory data and to compensate for errors on the axis of

the sensor accelerometer. Figure 2.7 shows the six different coordinate directions below.

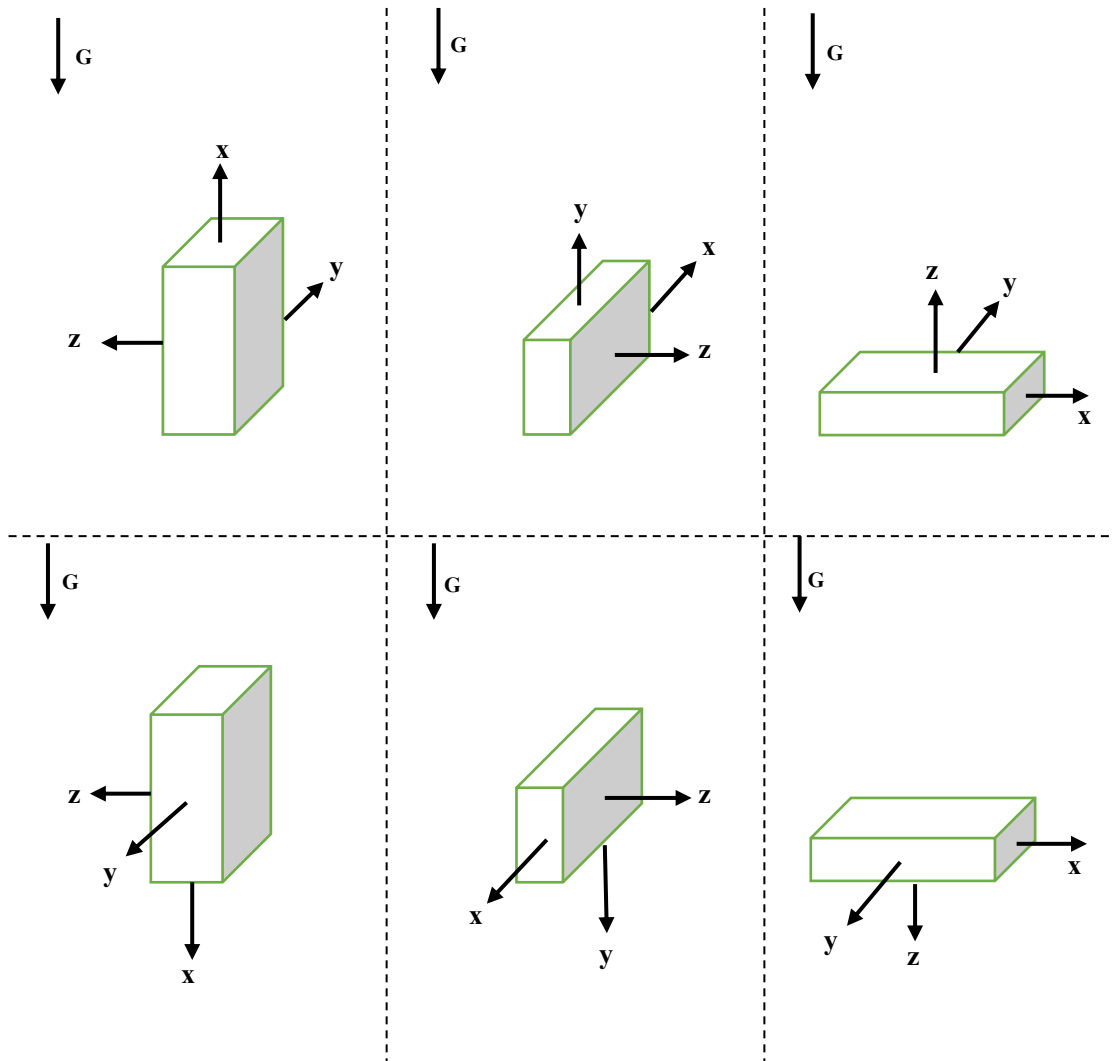
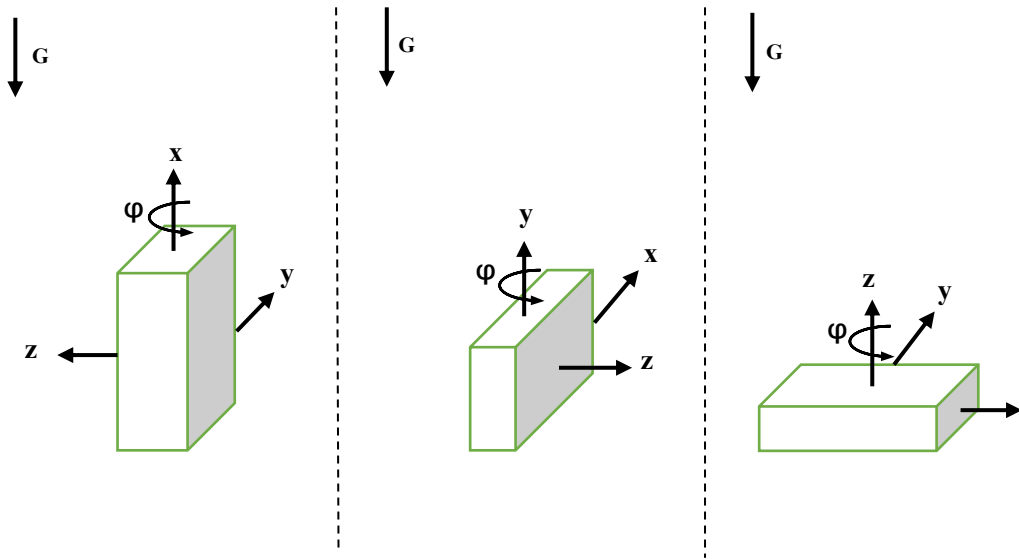


Figure 2. 7: Six-position static calibration method [52].

The gyroscope error model is similar to the accelerometer, and the calibration



**Figure 2. 8: Three-position calibration method.**

method adopted is three-position dynamic rotation. This involves placing the IMU in three different position as shown in Figure 2.8, making each axis rotate at the speeds of  $50^{\circ}/s$ ,  $100^{\circ}/s$ ,  $150^{\circ}/s$ ,  $200^{\circ}/s$ , and  $250^{\circ}/s$  in the up and down direction, and then collecting data. Compare the collected gyroscope data with the original factory data and perform error calibration.

In the IMU, the influence of the accelerometer is mainly reflected in the accuracy and stability of the accelerometer. Among them, the high accuracy of the accelerometer ensures the accuracy of subsequent data processing, and the stability of the accelerometer is a key factor directly affecting the normal performance of the IMU. The influence of the gyroscope on the IMU is mainly reflected in its accuracy, which will directly affect the performance of the attitude calculation. In other words, whether the IMU can correctly perceive the attitude of the product depends on the accuracy of the gyroscope.

Therefore, to ensure that, after the pedestrian wears the device, the coordinate system of the IMU sensor can be the same as the foot, the third step is to calibrate the accelerometer and gyroscope of the foot-mounted device after the pedestrian finishes

wearing it. When the device was worn, the bias of the IMU sensors was determined during zero movement scenarios. In a stationary situation, the reference output value of the X-axis and Y-axis of the accelerometer is zero, and the reference output value of the Z-axis of the accelerometer is the acceleration of gravity. For the X, Y, and Z axes of the gyroscope, the expected output in the static state is all 0. By collecting the data of pedestrians standing still on the ground for 10 s, the collected data are compared with the expected output values of the accelerometer and gyroscope. For a 100 Hz collection frequency device, 10,000 data sets can be collected within 10 s, which is sufficient for calibration. This method can effectively calibrate for the position error caused by pedestrians wearing the device.

The fourth step is to determine the noise error of the IMU sensor. The IMU sensor will be affected by noise, so a low signal-to-noise ratio will cause insensitivity of IMU. Therefore, for subsequent noise reduction processing, the initial noise variables based on the IMU sensor specification need to be determined. Table VI shows the initial noise variables for the LSM9DS1 IMU sensor, used for the PDR system in this thesis.

<b>TABLE VI</b>		
<b>Noise Type</b>	<b>Noise Value</b>	<b>Unit</b>
Accelerometer noise	0.05	$m/s^2$
Gyroscope noise	0.01	$rad/s$
ZUPT measurement noise	0.01	$m/s$

**Table VI: Initial Noise Variables.**

After completing the calibration steps, we can use the IMU sensor for more accurate data collection and to perform calculation processing by analyzing the changes in the data collected when the pedestrian is walking in order to estimate the walking trajectory of the pedestrian.

## 2.3 Data Expression

The Raspberry Pi connects to the IMU sensor via SSH and uses the i2c communication protocol to collect all data. The collected data includes all accelerometer axis and gyroscope axis values after the pedestrian starts the walk test. The collected data is saved in CSV format, and is then imported into MATLAB, where the algorithms defined herein are implemented. Table VII below shows the data collected from the IMU sensor directly and saved in the CSV file.

TABLE VII						
Time Stamp (s)	Accelerometer ( $m/s^2$ )			Gyroscope ( $rad/s$ )		
	Accel X	Accel Y	Accel Z	Gyro X	Gyro Y	Gyro Z
0.41237	1.05341	0.11004	9.92991	-0.01407	0.05586	-0.02228
0.42065	1.02538	0.13732	9.94334	-0.01233	0.06275	-0.02415
0.42917	1.03239	0.07857	9.92869	-0.01663	0.07469	-0.02538
0.43771	1.04640	0.09116	9.91647	-0.01485	0.08127	-0.0263
0.4462	0.95066	0.09535	9.95433	-0.0146	0.08534	-0.02419
0.45449	0.87360	0.10584	9.97632	-0.01826	0.07973	-0.02512
0.46305	0.81288	0.07647	10.0019	-0.01405	0.06761	-0.02153
0.47159	0.81055	0.07857	9.97632	-0.01261	0.05629	-0.02071
0.47987	0.82923	0.08066	9.96535	-0.01059	0.04255	-0.01826
0.48847	0.81522	0.09745	9.97266	-0.00571	0.02667	-0.01521
0.49679	0.86192	0.14781	9.94334	0.00052	0.01415	-0.01643
0.50535	0.91329	0.12682	9.93357	0.00742	0.01383	-0.01857
0.51388	0.93431	0.08277	9.93479	0.00681	0.01078	-0.01887
0.52219	0.88761	0.09745	9.96410	0.00773	0.00773	-0.01735
0.53077	0.86893	0.12473	9.95678	0.01172	0.00345	-0.01582
0.54773	0.90398	0.11424	9.94579	0.01200	-0.00113	-0.01887

Table VII: Data Samples Collected from IMU Sensor in CSV File.

To better summarize the relationship between the data collected by the sensors and the gait changes of pedestrians walking, this paper selects a 25 s period of walking data for analysis and explanation. In this 25 s walking experiment, the walker wore a device and, after the experiment started, stood still on the ground for 1.7 s, then started walking at the speed around 3 km/h, trying to maintain the same walking state throughout the experiment to collect acceleration and angular velocity data through the IMU sensor. The data collected through the experiment is shown in Figure 2.9 and 2.10. Figure 2.9 is the data collected by the accelerometer of the IMU sensor. It is composed of the data for the X-, Y-, and Z-axes of accelerometer. The X-axis and Y-axis in the accelerometer are calibrated to parallel to the ground, so the initial acceleration reading starts from 0. Since the Z-axis is perpendicular to the ground, the acceleration reading of the Z-axis starts from the gravity value. Figure 2.10 is the data collected by the gyroscope in the IMU sensor. It is also composed of data on the three axes – X, Y, and Z. At the beginning of the experiment, the pedestrian’s feet are stationary on the ground, so the angular velocity readings of the three axes all start from 0 rad/s. It can be seen from these two figures that, with the advancement of time, the graphics follow the same changing loops, from a stable state to a fluctuating state, regularly switching back-and-forth between the two.

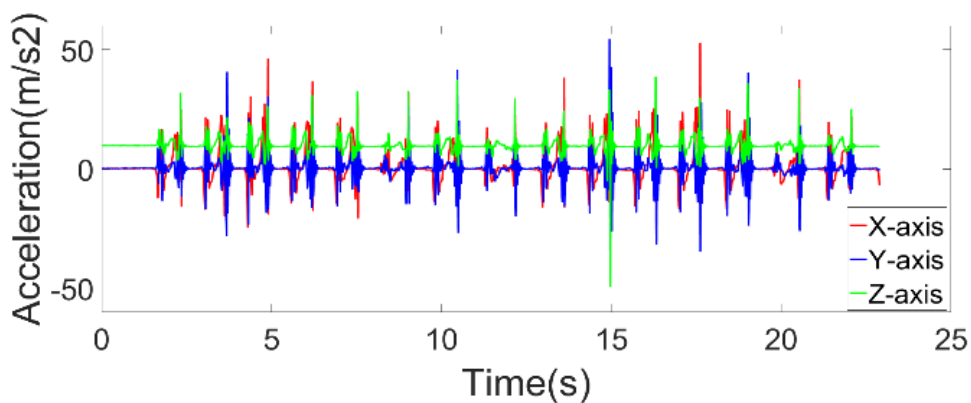


**Figure 2. 9: Acceleration data collected from 25 s walking test.**



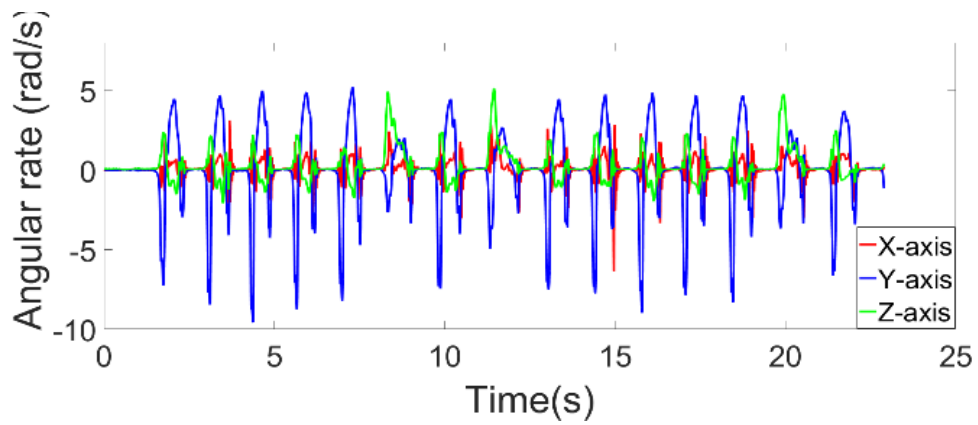


Figure 2. 10: Gyroscope data collected from 25 s walking test.

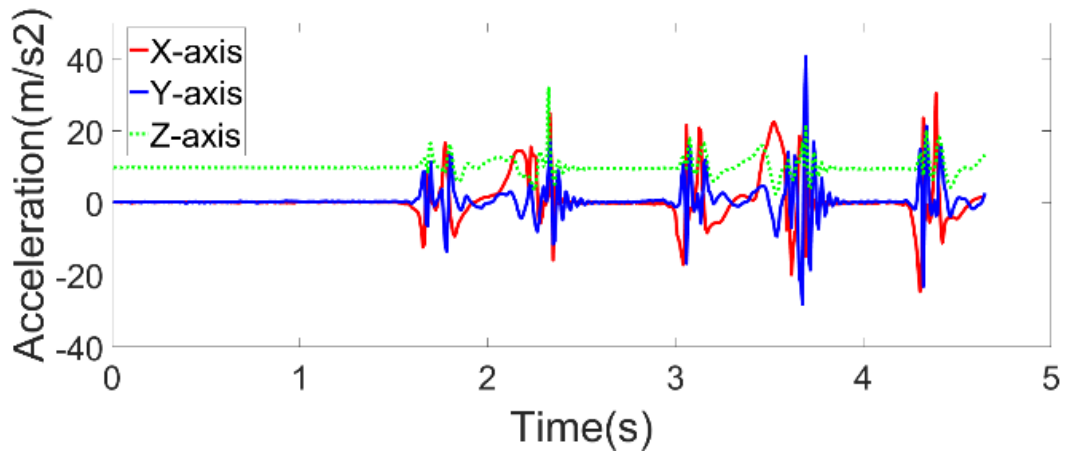
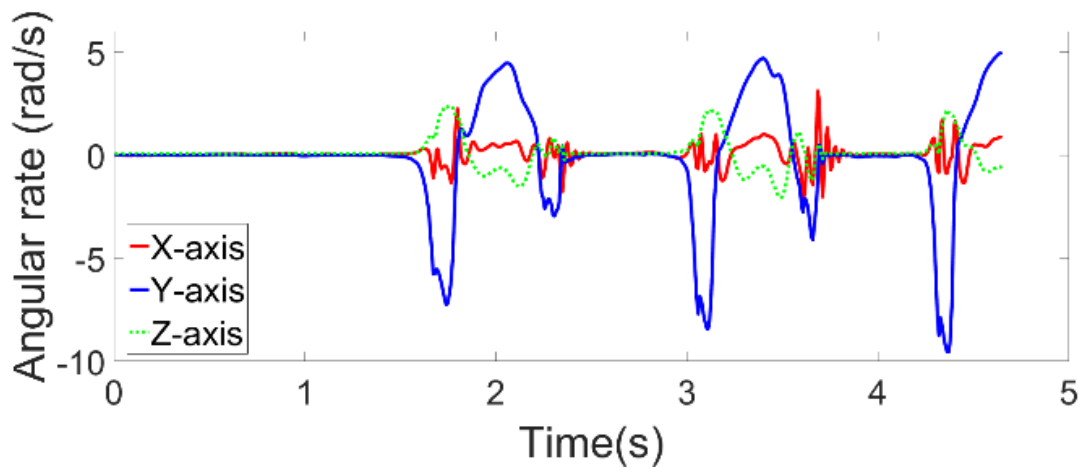


Figure 2. 11: The first 5 s acceleration data collected from 25 s walking test.

Figure 2.11 and Figure 2.12 are the experimental data figures for the first 5 s of the 25 s experiment. These two pictures make it clearer and more intuitive to see the relationship between gait transitions and data changes during walking.



**Figure 2. 12: The first 5 s gyroscope data collected from 25 s walking test.**

The accelerometer and gyroscope data collected by the IMU sensor is the basis of the entire PDR system. Only when the acceleration and angular velocity at each moment are accurately collected can the path estimation be performed by the INS algorithm. Moreover, the filter algorithm is also based on the accelerometer and gyroscope values, especially the ZUPT method.

Now, the design of the foot-mounted device and the calibration of the accelerometer and gyroscope of the IMU sensor have been completed, and the collection of the moment data on the X, Y, and Z axes have been finished after the calibration. Next, the algorithm of the PDR system needs to be developed.

## 2.4 Methodology and Implementation

### 2.4.1 Inertial Navigation System Algorithm

As seen in the basic PDR navigation system algorithm flowchart, the INS phase is the beginning of the entire PDR algorithm. It is mainly composed of two key parts; the first part is the conversion of orientation, and the second part is the calculation of

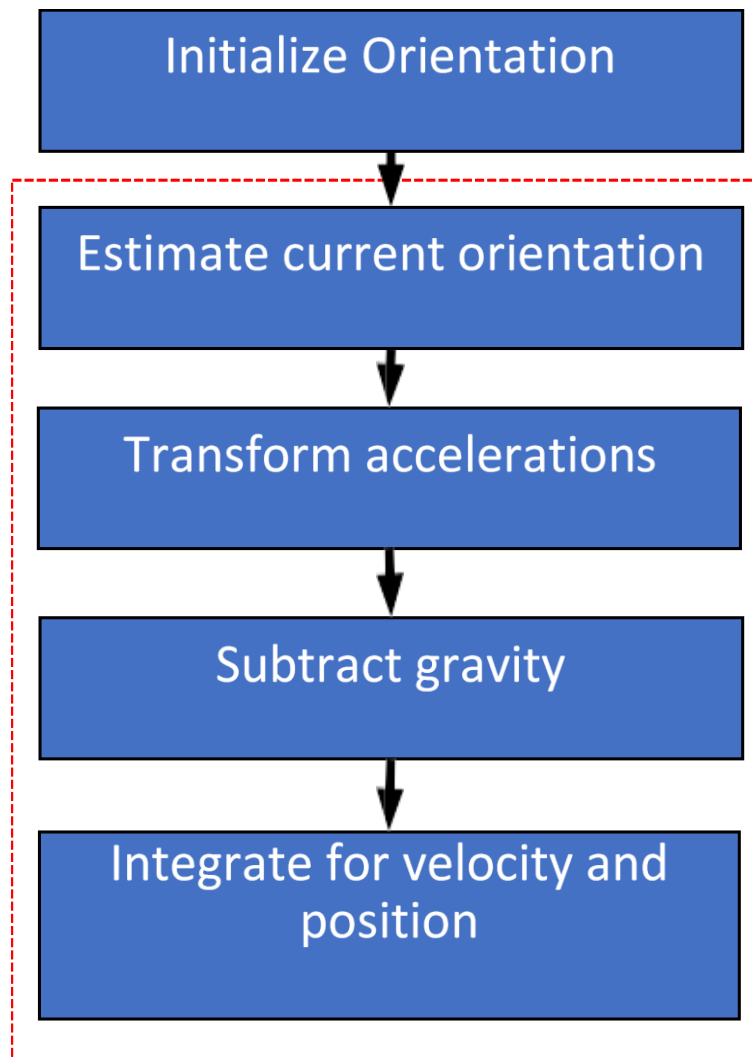


Figure 2. 13: Flowchart of the INS phase implementation algorithm.

velocity and position. The Figure 2.13 shows the flowchart of the INS phase implementation algorithm.

Because the IMU sensor has its own built-in orientation, the data collected by the IMU sensor is based on the orientation of the sensor itself. Therefore, when the collected data needs to be processed in the navigation direction in MATLAB, these two directions need to be unified. Only after finishing this step can the collected data be used in path estimation.

After completing the unification of orientation, the INS phase will integrate the acceleration data collected by the IMU sensor. Integrate the acceleration to get the velocity value and perform an integral calculation again on the velocity value to get the position. The position obtained by this method can be said to be the prototype algorithm of the PDR system. The formulas for the integration are shown below:

$$ds = v dt \quad (2.1)$$

$$s = \int_{t_1}^{t_2} v dt \quad (2.2)$$

$$s = \int_{t_1}^{t_2} \alpha t dt \quad (2.3)$$

Where  $\alpha$  is the acceleration,  $s$  is the displacement,  $t_1$  and  $t_2$  are the time stamp. The velocity is  $v = \alpha t$ .

Because there is error in the collected IMU sensor data, when the displacement obtained by this algorithm is combined with the angular velocity, there is heading drift. Therefore, the PDR system needs a basic filter algorithm to perform error processing on the results calculated in the INS phase. Generally, the filter system of the traditional PDR system is composed of a Kalman filter and the ZUPT method.

#### **2.4.2 Kalman Filter Algorithm**

A Kalman filter is an optimal estimation method based on variance. The Kalman filter algorithm in the PDR system is divided into two parts, the first being the prediction phase and the second being the correction phase.

In the prediction phase, there are two main formulas:

$$X(k|k-1) = AX(k-1|k-1) + BU(k) \quad (2.4)$$

Where A and B are matrix coefficients.  $X(k|k-1)$  is based on the results of the previous round of predictions.  $X(k-1|k-1)$  is the optimal prediction result in the previous round.  $U(k)$  is the control quantity of the current state. Through the first formula, the previous set can be verified and predicted based on the optimal value estimated, then the covariance of the error on the currently predicted data set can be calculated.

$$P(k|k-1) = AP(k-1|k-1)AT + Q \quad (2.5)$$

Where  $P(k|k-1)$  is the covariance of  $X(k|k-1)$ , and  $P(k-1|k-1)$  is the covariance of  $X(k-1|k-1)$ .  $Q$  is the error covariance of the estimation process. After completing the first part of the prediction phase, then the data can be corrected.

In the second phase, there are three main formulas. The first one is to calculate the Kalman gain:

$$K_g(k) = \frac{P(k|k-1)HT}{HP(k|k-1)HT + R} \quad (2.6)$$

Where the H is the coefficient matrix, and R is the noise covariance of the measured value. After the Kalman gain is calculated, a correction can be performed on the predict values:

$$X(k|k) = X(k|k-1) + K_g(k)(Z(k) - HX(k|k-1)) \quad (2.7)$$

Where  $Z(k)$  is the measured value.

$$P(k|k) = (I - K_g(k)H)P(k|k-1) \quad (2.8)$$

Where  $I$  is the identity matrix. This formula is used to update the error covariance.

The above five formulas constitute the basic working principle of the Kalman filter. When these formulas are applied to actual experiments, it is necessary to transform the variables in the formulas according to the actual situation. The following section will introduce how to establish a Kalman filter algorithm in the PDR system based on the data collected from the IMU sensor.

### **2.4.3 Zero-Velocity Update Algorithm**

Zero-velocity update method (ZUPT) is widely used in inertial measurement unit (IMU)-based pedestrian navigation systems for mitigating sensor drifting error. In the PDR algorithm, after the KF phase finishes estimating error covariance, the algorithm will enter the ZUPT detect phase. First, ZUPT will judge the walking state of the pedestrian. If the pedestrian is in the stance phase, a Kalman filter will start to estimate errors in velocity, position, and orientation, and then the algorithm will correct error covariance. The more accurate the pedestrian phase is, the more accurate the follow-up Kalman filter will be.

Judgment of the walking phases of pedestrians is based on thresholds obtained through experiments. Thresholds are the most important data in the ZUPT method; they are the basis of the entire ZUPT detection. The threshold value of each state when the gait changes is calculated by collecting the walking data of pedestrians and summarizing the data changes in the gait transition.

In the threshold experiments, people wear devices and perform walking experiments, which include normal walking, fast walking, climbing, and jumping, then data is collected. Classify different types of walking styles, perform one-to-one correspondence with the data, and take the maximum and minimum values of the data as the threshold of the walking style. For example, in the fast-walking experiment, the IMU data (acceleration data and angular velocity data) under fast walking condition is collected and plotted on the 2D coordinate system (Figure 2.14). The changing rule of the data is analyzed, and the maximum and minimum values of the stance phase and swing phase are used as the threshold for this segment data of fast walking. Through over 20 repetitions of the experiments, the applicable fast-walking threshold can be obtained.

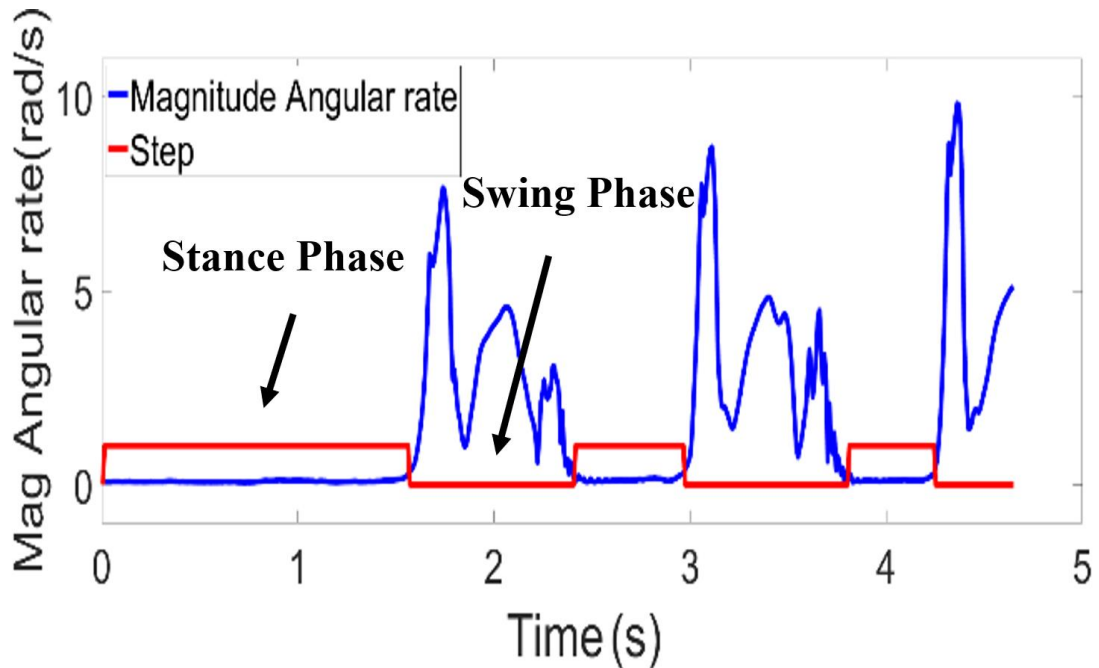


Figure 2. 14: Stance phase and swing phase shown by the magnitude angular rate.

The threshold value is calculated and summarized, and a list of the threshold value range of the ZUPT method experiment is obtained.

Angular rate value threshold:

$\omega_{threshold} = 0.6 \text{ rad/s}$ , when  $\omega_{threshold}$  value is smaller than 0.6 rad/s, the foot is in stance phase.

Accelerometer threshold shown in Table VIII:

<b>TABLE VIII</b>	
Motion State	Accelerometer Threshold (g)
Normal walking (3km/h - 4 km/h)	$a_{mag\_max} - a_{mag\_min} < 3g$
Fast walking (4 km/h – 6 km/h)	$3g < a_{mag\_max} - a_{mag\_min} < 4g$
Climbing stairs	$4g < a_{mag\_max} - a_{mag\_min} < 7g$
Striding or jumping	$a_{mag\_max} - a_{mag\_min} > 7g$
<p><math>g</math> is the gravity acceleration values.</p> <p><math>a_{threshold} = a_{mag\_max} - a_{mag\_min}</math></p> <p><math>a_{mag\_max}</math> is the maximum magnitude of the acceleration data</p> <p><math>a_{mag\_min}</math> is the minimum magnitude of the acceleration data</p>	

**Table VIII: Specific judgment of the accelerometer threshold.**

All thresholds used in this paper are calculated based on the IMU sensor used in this paper. To adapt the walking state of different pedestrians, the number of people in the threshold experiment is 20. 20 is not an ideal sample size, due to the limitations at the time of this thesis, this thesis cannot carry out larger-scale data collection and cannot provide more groups' sample test data as a reference for the threshold range. Therefore, if want a more accurate threshold range, to conduct further sample data collection and analysis is needed.

When the range of different motion threshold is determined, it can help the ZUPT method to determine the gait of pedestrians and reduce positioning errors more accurately. Next, the conventional single-threshold ZUPT method will be used to merge with the Kalman filter to construct an algorithm for the PDR system.



## 2.4.4 IMU-Based PDR Algorithm

Because it is an IMU-based PDR algorithm, the data collected are the accelerometer value, gyroscope value, and time stamp. According to the IMU sensor used, some variables also need to be initialized at the beginning of the algorithm:

System initialized parameter values shows in the Table IX [25]:

TABLE IX	
System Initialized Parameter	Values
Gravity	$g = 9.8 \text{ m/s}^2$
Time step	$\Delta t = 0.01 \text{ second (100Hz)}$
Acceleration matrix	$a = (0_x \ 0_y \ 0_z)^T$
Velocity matrix	$V = (0_x \ 0_y \ 0_z)^T$
Position matrix	$P = (0_x \ 0_y \ 0_z)^T$
KF error covariance matrix	$p = 0_{9 \times 9}$
ZUPT acceleration threshold: $\sigma_{ta}$ ZUPT gyroscope threshold: $\sigma_{t\omega}$	

Table IX: System initialized parameter values.

Initialize the acceleration orientation matrix  $C_k$ :

$$C_k = \begin{bmatrix} \cos(\text{pitch}) & \sin(\text{roll}) \sin(\text{pitch}) & \cos(\text{roll}) \sin(\text{pitch}) \\ 0 & \cos(\text{roll}) & -\sin(\text{roll}) \\ -\sin(\text{pitch}) & \sin(\text{roll}) \cos(\text{pitch}) & \cos(\text{roll}) \cos(\text{pitch}) \end{bmatrix}, \quad (2.9)$$

$$\text{roll} = \arctan\left(\frac{a_y^{\text{sensor}}}{a_z^{\text{sensor}}}\right) \quad (2.10)$$

$$\text{pitch} = -\arcsin\left(\frac{a_x^{\text{sensor}}}{\text{gravity}}\right) \quad (2.11)$$

$$\text{yaw} = 0 \quad (2.12)$$

Roll, pitch, and yaw are the three basic variables to calculate in the orientation

matrix  $C_k$ ; these three variables are calculated from the IMU acceleration data.

The IMU sensor will be affected by noise, so use the initial noise variables shown in Table VI:

Accelerometer noise:  $\sigma_a = 0.05 \text{ m/s}^2$

Gyroscope noise:  $\sigma_\omega = 0.01 \text{ rad/s}$

ZUPT measurement noise:  $\sigma_v = 0.01 \text{ m/s}$

Acceleration noise covariance as a diagonal matrix with values:

$$R_a = \text{diag} (\sigma_{a,x} \ \sigma_{a,y} \ \sigma_{a,z})^2 \quad (2.13)$$

Gyroscope noise covariance as a diagonal matrix with values:

$$R_\omega = \text{diag} (\sigma_{\omega,x} \ \sigma_{\omega,y} \ \sigma_{\omega,z})^2 \quad (2.14)$$

ZUPT measurement noise covariance as a diagonal matrix with values:

$$R_z = \text{diag} (\sigma_{v,x} \ \sigma_{v,y} \ \sigma_{v,z})^2 \quad (2.15)$$

After completing the creation of the initial value, the algorithm can be built for the PDR system. The algorithm built is based on the principles of INS phase, KF phase, and ZUPT phase [25].

First, the data collected by the gyroscope in the IMU sensor needs to subtract the bias error, the bias error should be calculated by the data at the beginning of the experiment:

$$\omega = \omega - \omega_{bias} \quad (2.16)$$

Then, the skew-symmetric angular rate matrix is calculated, and the orientation matrix in sensor frame is updated:

$$\Omega_k = \begin{bmatrix} 0 & -\omega_z & \omega_y \\ \omega_z & 0 & -\omega_x \\ -\omega_y & \omega_x & 0 \end{bmatrix} \quad (2.17)$$

$$C_k = C_{k-1} = \frac{2I_{3 \times 3} + \Omega_k \Delta t}{2I_{3 \times 3} - \Omega_k \Delta t} \quad (2.18)$$

Because the orientation frame of the sensor is different from the navigation frame of pedestrian, the sensor frame data need to be converted to navigation frame data. The next step is to transfer the measured accelerations from the sensor frame to navigation frame and to calculate the skew-symmetric acceleration rate matrix, which shows the changes in velocity and orientation errors:

$$a_k^{nav} = \frac{(C_k + C_{k-1})a_k^{sensor}}{2} \quad (2.19)$$

$$A_k = \begin{bmatrix} 0 & -a_z & a_y \\ a_z & 0 & -a_x \\ -a_y & a_x & 0 \end{bmatrix} \quad (2.20)$$

After the navigation frame acceleration  $a_k^{nav}$  is determined, take the integrate calculation to obtain the estimated velocity:

$$V_k = V_{k-1} + \frac{(a_k^{nav} + a_{k-1}^{nav} - 2(0 \ 0 \ g)^T)\Delta t}{2} \quad (2.21)$$

After the velocity is determined, the position can be estimated by:

$$P_k = P_{k-1} + \frac{t}{2}((V_k + (V_{k-1})) \quad (2.22)$$

Update the error covariance matrix:

$$p_k = F_k p_{k-1} F_k^T + R_a R_\omega \Delta t \quad (2.23)$$

$$F_k = \begin{bmatrix} I_{3 \times 3} & 0_{3 \times 3} & 0_{3 \times 3} \\ 0_{3 \times 3} & I_{3 \times 3} & I_{3 \times 3} \Delta t \\ -A_k \Delta t & 0_{3 \times 3} & I_{3 \times 3} \end{bmatrix} \quad (2.24)$$

Detect the stance phase or swing phase:

$$\omega_k \leq \sigma_{t\omega} \text{ (stance phase)} \quad (2.25)$$

Compute the Kalman gain  $K_k$ :

$$K_k = p_k H^T (H p_k H^T + R_Z)^{-1} \quad (2.26)$$

H is the zero-velocity measurement matrix:

$$H = (0_{3 \times 3} \ 0_{3 \times 3} \ I_{3 \times 3}) \quad (2.27)$$

Compute the state error from Kalman gain  $K_k$ :

$$\varepsilon_k = K_k V_k = (\varepsilon_C \varepsilon_P \varepsilon_V)^T \quad (2.28)$$

$\varepsilon_C$  is the complete error vector of attitude,  $\varepsilon_P$  is the complete error vector of position,  $\varepsilon_V$  is the complete error vector of velocity.

To show the complete error vector in the matrix:

$$\varepsilon_C = (\varepsilon_{C,1} \ \varepsilon_{C,2} \ \varepsilon_{C,3})^T \quad (2.29)$$

$\varepsilon_{C,1}$  is roll error value,  $\varepsilon_{C,2}$  is pitch error value, and  $\varepsilon_{C,3}$  is yaw error value.

$$\varepsilon_P = (\varepsilon_{P,1} \ \varepsilon_{P,2} \ \varepsilon_{P,3})^T \quad (2.30)$$

$$\varepsilon_V = (\varepsilon_{V,1} \ \varepsilon_{V,2} \ \varepsilon_{V,3})^T \quad (2.31)$$

After the H and  $K_k$  are both determined, the error covariance can be corrected:

$$p_k = (I_{9 \times 9} - K_k H) p_k \quad (2.32)$$

And correct the velocity estimate and position estimate:

$$V_k = V_k - \varepsilon_V \quad (2.33)$$

$$P_k = P_k - \varepsilon_P \quad (2.34)$$

$$C_k = \frac{2I_{3 \times 3} + \Omega_{\varepsilon k}}{2I_{3 \times 3} - \Omega_{\varepsilon k}} C_k \quad (2.35)$$

$$\Omega_{\varepsilon k} = \begin{bmatrix} 0 & \varepsilon_{C,3} & -\varepsilon_{C,2} \\ -\varepsilon_{C,3} & 0 & \varepsilon_{C,1} \\ \varepsilon_{C,2} & -\varepsilon_{C,1} & 0 \end{bmatrix} \quad (2.36)$$

After completing the PDR algorithm, the data collected by the IMU sensor can be imported for pedestrian route estimation. The data selected for the test is the 25 s walking test data used in the data expression section. The next page will display and compare, based on the INS stage algorithm, the output results of the system that does not include the KF stage and the ZUPT stage, as well as the output results after adding these two stages.

## 2.5 Map Plots of Basic PDR Algorithms

To facilitate the analysis of the calculation and estimation results of each part of the PDR algorithm, only the PDR system based on the INS algorithm is used to first draw the 25 s of data and see what kind of graph will be obtained. The Figure 2.15 below is the one obtained from MATLAB. Test 25 s data on a rectangular indoor area of 5 m \* 1.5 m.

Figure 2.15 shows the estimated path on a map. The blue line represents the estimated pedestrian walking route. The testing area is a rectangular area, but the path shown by the plot has serious drifting error. Therefore, in the case of only the INS phase

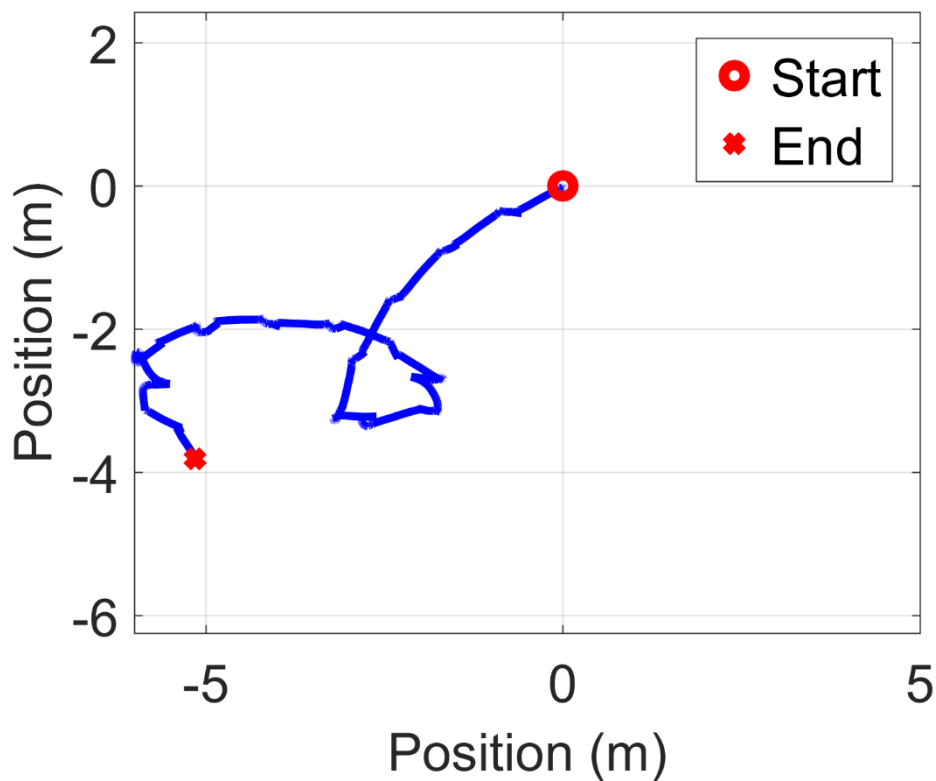
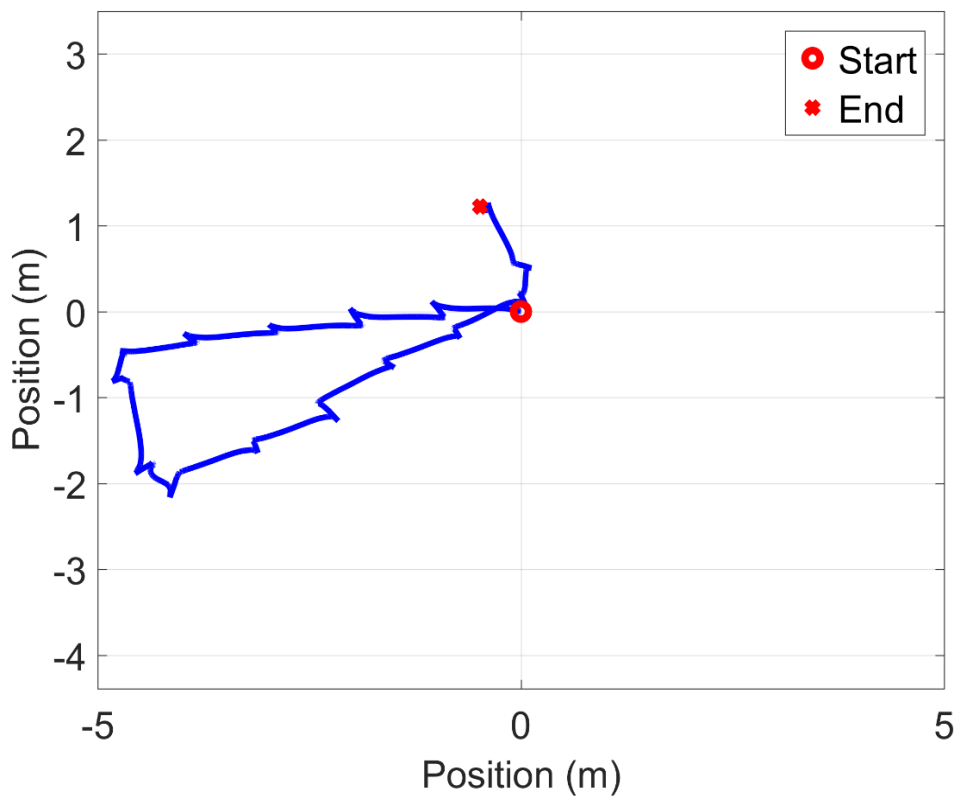


Figure 2. 15: Estimated walking path for 25 s based on INS phase algorithm only.

algorithm, the PDR system does not have precise navigation functions and cannot effectively correct the errors.

Next, a Kalman filter and a single-threshold ZUPT method were added to the PDR algorithm, and the same data was used to draw a path diagram in MATLAB. The Figure 2.16 below shows the figure obtained from MATLAB. As can be seen from Figure 2.16, due to the addition of the filter and the conventional single-threshold ZUPT method, the drift of the pedestrian's walking path has been greatly improved compared with the previous figure. The tested area is rectangular, and, this time, the PDR system maintains a good walking shape in the first straight line and the first corner after the walking starts. Due to the accumulation of errors, however, drift occurred after the first corner. As a result, the system was unable to complete the accuracy path estimation and only forms a drift-shaped triangular route on the map.



**Figure 2. 16: Estimated walking path for 25 s based on INS phase algorithm with conventional single threshold ZUPT method.**

Comparing Figure 2.15 with Figure 2.16, after the KF filter and ZUPT method are added to the PDR system algorithm, the pedestrian trajectory becomes clearer. Although there are still drift errors, the overall shape of the pedestrian walking area can be roughly determined. To solve the drift error that still exists after the Kalman filter and the traditional ZUPT method were added to the PDR system, a solution is proposed: without changing the Kalman filter algorithm structure, it is planned to conduct a detailed analysis of the traditional ZUPT judgment and to try developing the conventional ZUPT methods and improving the accuracy of path estimation on the map.

## **2.6 Benchmark Summary**

After completing the device setup and calibration and completing the algorithm design of the basic PDR system, this thesis requires a benchmark for the further experiments, and compares the experimental results with the benchmark setup, summarizing the advantages and disadvantages of different methods.

At current stage, this thesis can use the basic KF phase and ZUPT phase to eliminate drifting errors in PDR's INS phase, and a certain error elimination ability is reflected in the results of the map plot in Figure 2.16. And the method used in Figure 2.16 is also the conventional method in this thesis. Therefore, this thesis will use this method device setup data and walking test result as the benchmark data, which will be used for the further experiment results' comparison.

Table X shows the benchmark data for different specifications of the IMU sensor and device setup used in this thesis. In the following algorithm redesign and experiment comparison, the benchmark will be used as a reference for experimental results for comparison and analysis.



<b>TABLE X</b>	
Motherboard	Raspberry pi 3B
IMU sensor	SparkFun LSM9DS1
Operating voltage	3.3 V
Operating frequency	100 Hz
Mounted type	Shoe-mounted
Acceleration noise	$0.05 \text{ m/s}^2$
Gyroscope noise	$0.01 \text{ rad/s}$
ZUPT measurement noise	$0.01 \text{ m/s}$
Algorithms	KF filter + single gyroscope threshold ZUPT method
Gravity	$g = 9.8 \text{ m/s}^2$

**Table X: Device benchmark data**

# **Chapter 3: Development of Pseudo-Zero Velocity Re-Detection Double Threshold Zero-Velocity Update Method**

## **3.1 Conventional ZUPT Methods**

### **3.1.1 Introduction to Two Conventional ZUPT Methods**

In this study, two conventional ZUPT methods were used, PDR walking experiments were carried out, and the performance of each method in the experiment was recorded.

The first conventional ZUPT method used is the single-threshold ZUPT method. This ZUPT method is based on the gyroscope threshold. The gyroscope threshold value is 0.6 rad/s, as mentioned in the previous section. The ZUPT method only uses one-threshold detection, and, based on the detection, the error correction of the pedestrian path is performed. Because of the limitations of single-threshold detection, it cannot accurately determine the zero-speed interval when pedestrians are walking, so the pedestrian's gait changes cannot be accurately analyzed.

The second method is based on the first method, adding the analysis of variance. Based on the threshold judgment, variance judgment is performed on the judged zero-velocity interval, which can effectively detect abrupt data, eliminating and compensating for misjudgment caused by errors.

Next, these two conventional methods will be tested separately, with analysis of the performance of these two methods in judging the zero-velocity intervals and comparison of the results to analyze the advantages and disadvantages of each.

### 3.1.2 Pseudo-Zero-Velocity Interval and False Detection

Because the error and noise of a low-cost IMU sensor is usually very high, these vibrations can easily cause errors and false detection in pedestrian walking and step data. Also, due to the impact of noise on the IMU, the conventional ZUPT cannot form continuous intervals. Additionally, due to the incompleteness of the threshold, the phase conversion interval is not correctly detected [55]. Although the variance can well maintain the stability of the data, the large calculation volume of the variance will overload the IMU sensor with work. To better compare the performance of different ZUPT methods, this paper uses the same 25 s pedestrian walking data for analysis.

As shown in Figure 3.1 and Figure 3.2, the data used this time is the relationship between magnitude acceleration and time. Figure 3.1 is the result of the conventional, single-threshold ZUPT, while Figure 3.2 is the conventional single threshold-with-variance ZUPT method's result, based on the listed gyroscope threshold. The ZUPT judged numbers are 10 and 0 (10 meaning the stable phase and 0 meaning the swing

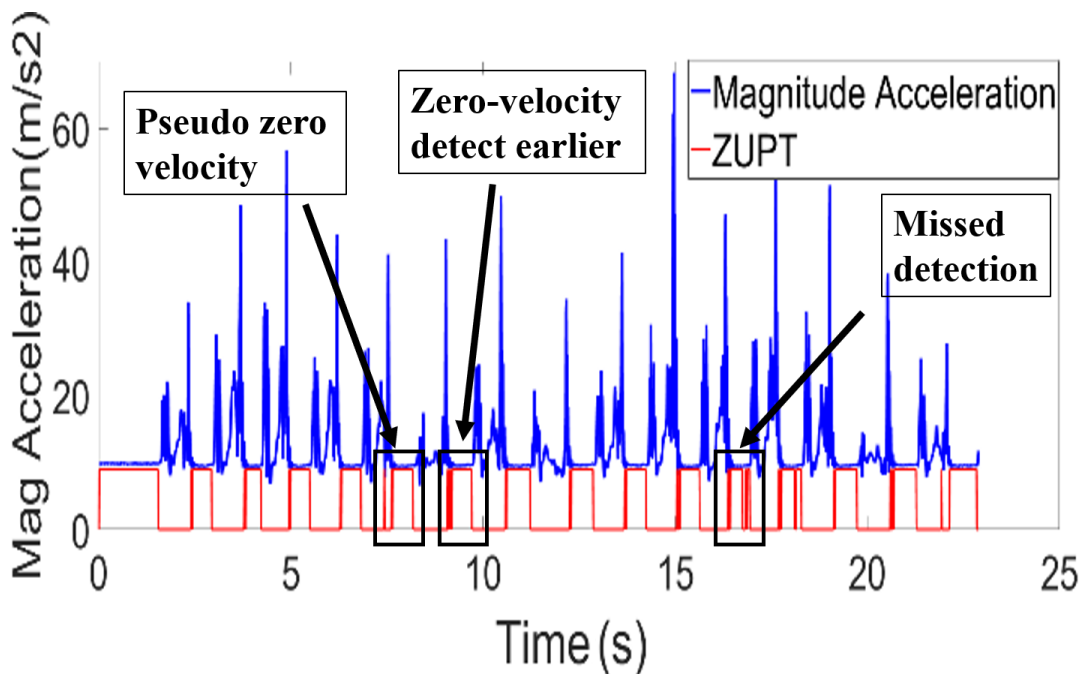


Figure 3. 1: Conventional method false detection of zero-velocity.

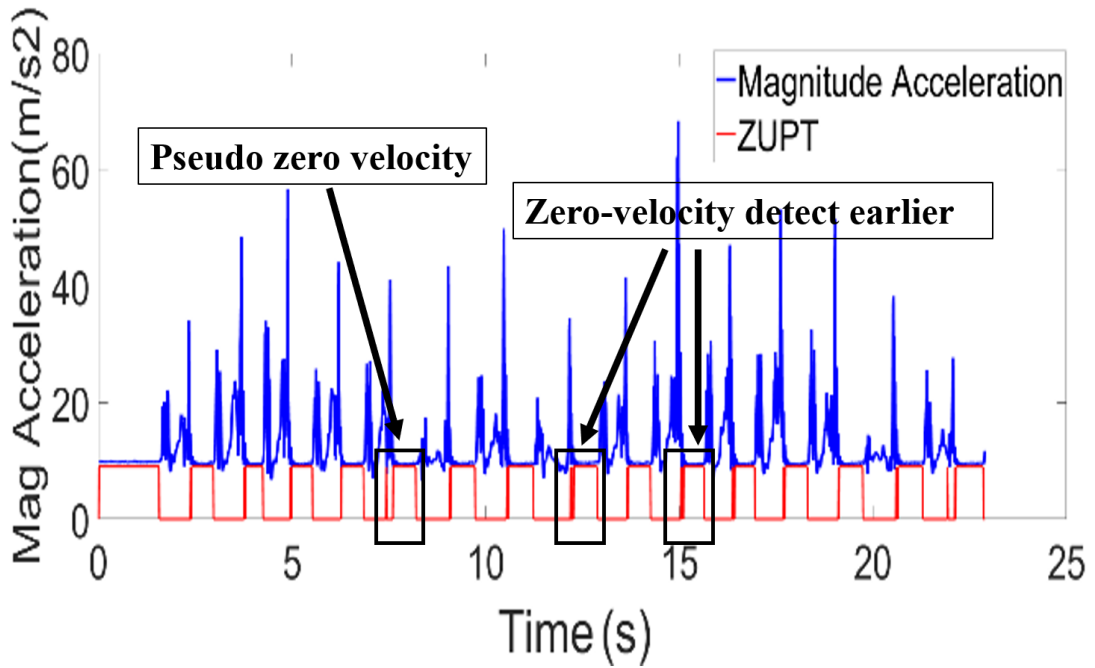


Figure 3. 2: Single-threshold-with-variance method false detection of zero-velocity.

phase). As shown in Figure 3.1, there are three black blocks, and the first is pseudo-zero velocity. In the first black block, there are two detected stance phase results: the first is a very short interval, and the second is the normal red interval block. Comparing it with the blue curve, we can see the second red block corresponding to the curve is at a stable level – the stance phase – so this is a correct detection. The first short red block corresponding to the blue curve, however, is still in swing phase, and the ZUPT detects this data as stance phase; this is a pseudo-zero-velocity interval. The second black block is zero velocity detected earlier. The red block has a thick line in the front because, when a pedestrian switches from swing phase to stance phase, there will be a buffer period. The data in the buffer period may meet the threshold detection conditions due to the influence of vibration, but it is not the stance phase. The third block is a missed detection. When the blue curve maintains a stable level, which means it is in stance phase, the red block is not continuous. This is also due to the influence of external factors. During the pedestrian's stance phase, the data will fluctuate and the condition of the ZUPT threshold is not met. It is judged to be the swing phase, so a continuous red block cannot occur.

Figure 3.2 shows the single-threshold-with-variance ZUPT method. The variance can better maintain the data in a stable level, so the non-continuous interval does not occur in the figure, but the pseudo-zero velocity and earlier detection cannot be better removed. In the swing phase, the data changes have always been in a relatively large state, so the variance cannot handle this part of the data, though it can play a good role in the relatively stable state of the stance phase data.

Figure 3.3 is the foot trajectory diagram in a 3D space coordinate system when the pedestrian is walking at a constant speed in the 25 s walking experiment. Figure 3.3 shows the step length of each step of the pedestrian, which is used to calculate the displacement of the pedestrian. To determine the number of steps when pedestrians are walking, it is necessary to accurately judge the stance phases and swing phases through ZUPT.

The determination of the zero-velocity interval can better recognize the pedestrian's phase changes during walking, and, by using the ZUPT method, the pedestrian's motion state can be divided into two parts – swing phase and stance phase. The two parts calculate the displacement and direction separately. If there is no way to accurately determine the zero-velocity interval, it is impossible to accurately use the pedestrian walking data to calculate the pedestrian's displacement and direction. Therefore,

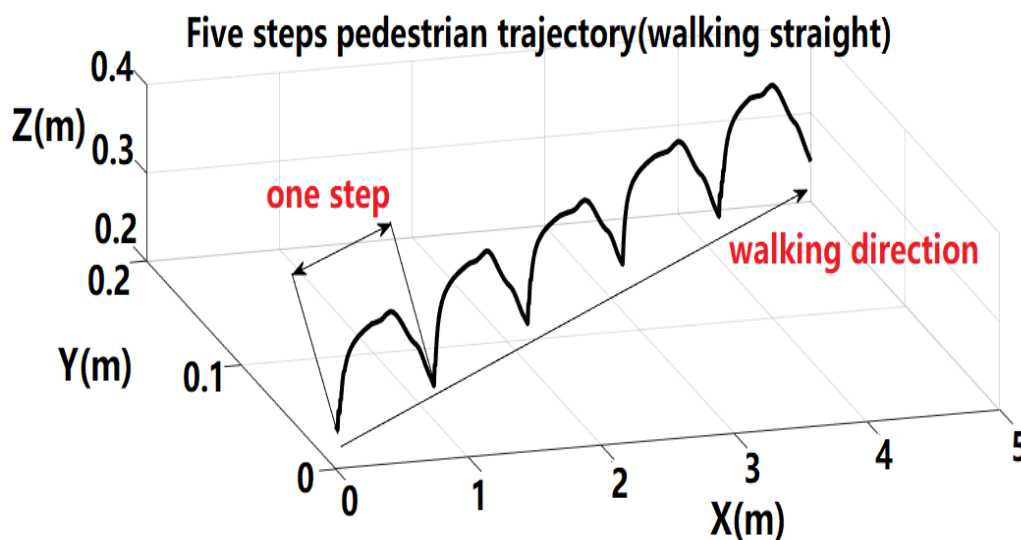


Figure 3. 3: Identification of pedestrian's foot 3D walking trajectory.

without the use of additional equipment, the conventional ZUPT method is redesigned to develop a more accurate ZUPT method, which can better help the PDR system eliminate errors generated during walking.

## **3.2 Pseudo-Zero-Velocity Re-Detection Double-Threshold ZUPT**

### **Method**

#### **3.2.1 Implementation Algorithm of Proposed ZUPT Method**

To better solve these existing problems, the proposed method can reduce the calculation steps, better remove pseudo-zero velocity, and account for the error effect caused by walking vibrations, thus improving the accuracy of the step count.

The following is the operating principle of this proposed method. The frequency of the IMU sensor used in the experiment is between 100 Hz and 120 Hz. To avoid the load operation of the IMU sensor, 100 Hz has been chosen as the basis frequency for experimental data collection, so the data collecting speed is limited at 100 sets per hour:

$$f = 100 \text{ Hz}$$

Table XI and Table XII show the data samples collected by three experimenters walking in two different speed ranges. Each sample represents a complete ZUPT judgment interval, which is a complete walking step. As the walking speed increases, the time of one step becomes shorter and the corresponding collected data decreases. Taking Table XII as an example, Pedestrian #1 needs 19 data to complete a stance phase, and the number of data needed to complete a swing phase is 27. Pedestrian #3, who has different running postures, needed 25 data to complete a stance phase, and 20 data to complete a swing phase. Compared with the speed of 3-4 km/h, more data is needed to complete the corresponding phase.

TABLE XI					
Pedestrian	Phase	Sub-Phase	Number of Data		Percentage
<b>1</b>	Stance	Full contact	32	58	41.1%
		Pre-swing	12		
		Pre-stance	14		
	Swing	Acceleration	43	83	58.9%
		Deceleration	40		
<b>2</b>	Stance	Full contact	43	67	44.1%
		Pre-swing	11		
		Pre-stance	13		
	Swing	Acceleration	48	85	55.9%
		Deceleration	37		
<b>3</b>	Stance	Full contact	64	98	59%
		Pre-swing	16		
		Pre-stance	18		
	Swing	Acceleration	37	68	41%
		Deceleration	31		

Table XI: The amount of data collected for foot phases at 3-4 km/h.

TABLE XII					
Pedestrian	Phase	Sub-Phase	Number of Data		Percentage
<b>1</b>	Stance	Full contact	12	19	41.3%
		Pre-swing	3		
		Pre-stance	4		
	Swing	Acceleration	15	27	58.7%
		Deceleration	12		
<b>2</b>	Stance	Full contact	13	22	48.8%
		Pre-swing	3		
		Pre-stance	6		
	Swing	Acceleration	10	23	51.2%
		Deceleration	13		
<b>3</b>	Stance	Full contact	14	25	55.3%
		Pre-swing	7		
		Pre-stance	4		
	Swing	Acceleration	12	20	44.7%
		Deceleration	8		

**Table XII: The amount of data collected for foot phases at 8-10 km/h.**

Next, we perform data analysis on the pseudo-zero-velocity interval and failed detection interval, as seen in Figure 3.1. Table XIII shows the results of ZUPT judgment from the 6th to the 10th second in Figure 3.1 and the amount of data in each phase result. From the phase conversion results in the table, there are two completely phase conversions within 7.4 s-7.5 s. The first is from 7.4 s to 7.43 s, which completes the conversion from swing phase to stance phase, and the second is from 7.43 s to 7.5 s, completing the conversion from stance phase to swing phase. According to the figure,



the data result in this time should be the pseudo-zero-velocity interval; moreover, by summarizing the walking habits of pedestrians, pedestrians cannot complete phase conversion within 3 or 7 data. From this, it can be judged that the phase conversion between 7.4 s-7.5 s does not exist, likely the result of errors. According to the previous phase state of 6.7 s-7.4 s, we can infer that 7.4 s-7.5 s should be a swing phase. Through multiple walking experiments and the judgment result of ZUPT, it can be concluded that, at a frequency of 100 Hz, pedestrians cannot complete a complete phase conversion within 10 data. Therefore, we choose 10 as the judgement threshold in the proposed ZUPT method.

<b>TABLE XIII</b>			
<b>Time</b>	<b>Data Samples</b>	<b>Phase Results</b>	<b>Corrected</b>
6.00 s-6.30 s	30	Swing	Swing
6.30 s-6.70 s	41	Stance	Stance
6.70 s-7.40 s	69	Swing	Swing
7.40 s-7.43 s	3	Stance	Swing
7.43 s-7.50 s	7	Swing	Swing
7.50 s-8.10 s	60	Stance	Stance
8.10 s-9.10 s	100	Swing	Swing
9.10 s-9.17 s	7	Stance	Swing
9.17 s-9.18 s	1	Swing	Swing
9.18 s-9.20 s	2	Stance	Swing
9.20 s-9.24 s	4	Swing	Swing
9.24 s-9.70 s	46	Stance	Stance
9.70 s-10.0 s	30	Swing	Swing

**Table XIII: ZUPT Detected results from 6 s-10 s.**

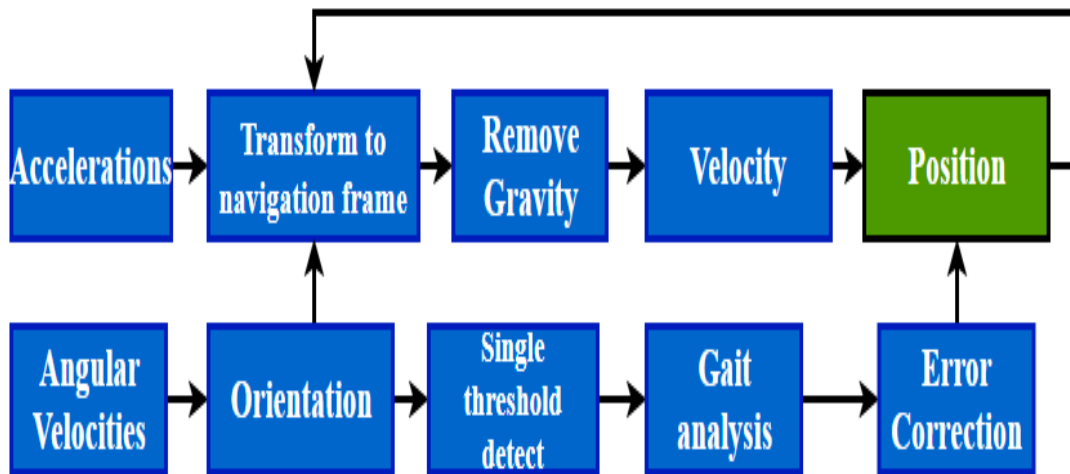


Figure 3. 4: Flowchart of the single-threshold ZUPT implementation algorithm [25].

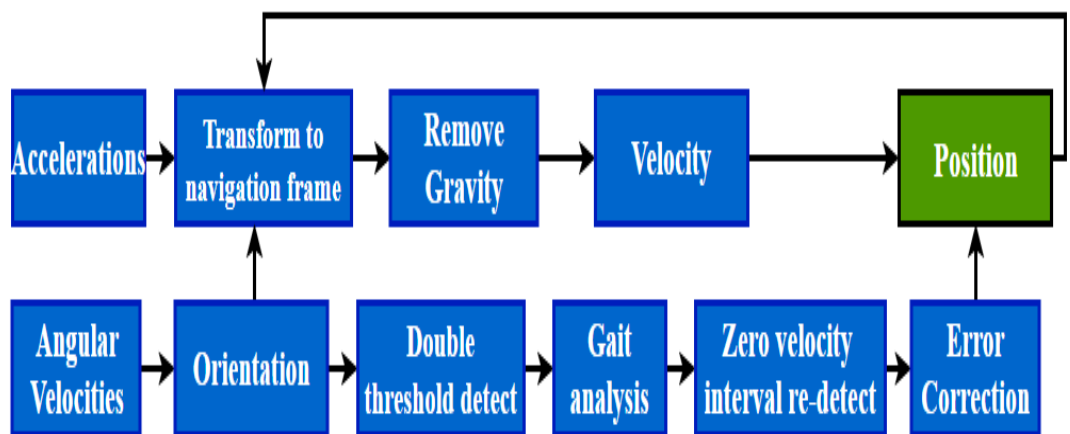


Figure 3. 5: Flowchart of the pseudo-zero-velocity re-detection double-threshold ZUPT implementation algorithm.

After determining 10 as the judgment threshold, we summarize the principle of the proposed ZUPT method and list the formula algorithm. Figure 3.4 shows the flowchart of the single threshold ZUPT implementation algorithm, while Figure 3.5 shows the pseudo-zero-velocity re-detection double-threshold ZUPT implementation algorithm. After ZUPT completes the first double threshold determination, the re-detection algorithm will re-detect the determined results.

### 3.2.2 The Formula Implementation Algorithm

Initialize the swing phase interval:

$$I_{sw,n} = [0_1, 0_2, 0_3 \dots 0_{n-1}, 0_n] \quad (3.1)$$

ZUPT judges that the data is in swing phase and is represented by the number 0.  $n$  represents the amount of data in the swing interval.

Initialize the stance phase interval:

$$I_{st,m} = [1_1, 1_2, 1_3 \dots 1_{m-1}, 1_m] \quad (3.2)$$

ZUPT judges that the data is in stance phase and is represented by the number 1.  $m$  represents the amount of data in the stance interval.

$$T_{data} = 10$$

$T_{data}$  is the re-detection interval size threshold. (For different  $T_{data}$  step detection test results are in chapter 4.1)

If one interval is formed in the double-threshold detection part, and it is determined as the swing phase interval, which is composed of  $n_1$  data:

$$I_{sw,n_1} = [0_1, 0_2, 0_3 \dots 0_{n_1-1}, 0_{n_1}]$$

Then re-detect this swing phase interval:

$$\text{whether } n_1 > T_{data} \quad (3.3)$$

If true, the judgment of the previous step is correct, which means the interval is a swing phase interval. So, keep the phase result and interval, and proceed to the next interval.

If the next interval – which formed in the double-threshold detection part – is determined as the stance phase interval, and is composed of  $m_1$  data:

$$I_{st,m_1} = [1_1, 1_2, 1_3 \dots 1_{m_1-1}, 1_{m_1}]$$

Then re-detect this stance phase interval:

$$\text{whether } m_1 > T_{data} \quad (3.4)$$

If false, the judgment of the previous detection is incorrect. Then convert the stance phase interval into the swing phase interval, and combine it with the previous swing phase interval:

$$I_{sw,n_1} = I_{sw,n_1+st,m_1} = [0_1, 0_2, 0_3 \dots 0_{(n_1+m_1)-1}, 0_{n_1+m_1}] \quad (3.5)$$

After completing the new ZUPT method algorithm, this 25 s of data will be re-analyzed, and the estimated pedestrian's trajectory will be plotted by using this new algorithm; the performance of this new ZUPT method in judging zero-velocity intervals will be compared with the two conventional ZUPT methods. For the selection of  $T_{data}$  value, there is a detailed analysis in the step detection test of Chapter 4.1.

### 3.2.3 New ZUPT Method's Performance and Testing Results

Through this proposed ZUPT method, all intervals can be re-detected, and the interval with errors can be corrected, which improves the accuracy of ZUPT judgment. As shown in Figure 3.6, our proposed ZUPT method solves the problem that the pseudo-zero-velocity interval cannot be detected correctly, removes the early false detection, and makes every detected phase interval a continuous interval.

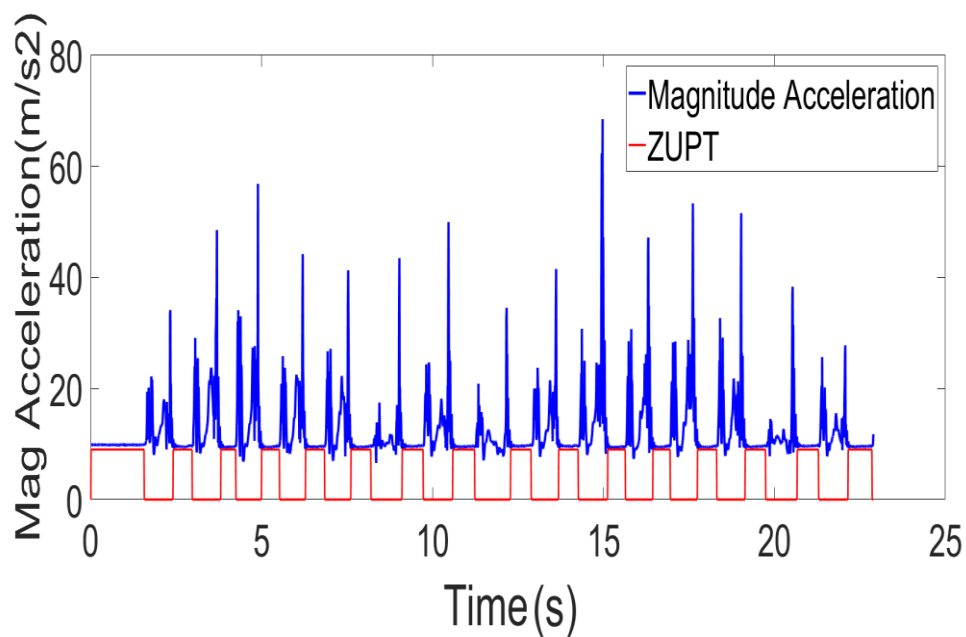


Figure 3. 6: The proposed ZUPT method with no false detection.

The proposed ZUPT method has excellent performance in the detection of pedestrian stance phase and swing phase. Next, we need to test whether the detection result can help the PDR system to improve the accuracy of the pedestrian walking path in the navigation map. The PDR system is used in conjunction with the proposed ZUPT method algorithm to replot the 25 s data on the map. Figure 3.7 below shows the estimated path map from MATLAB.

As can be seen from Figure 3.7, the tested 5 m \* 1.5m rectangular indoor area can be better estimated on the map plot. This walking path has the closest similarity to the ground truth. Therefore, comparing the results of a PDR system with a single-threshold ZUPT method, the proposed ZUPT method can significantly improve the accuracy of the PDR system in estimating the walking path.

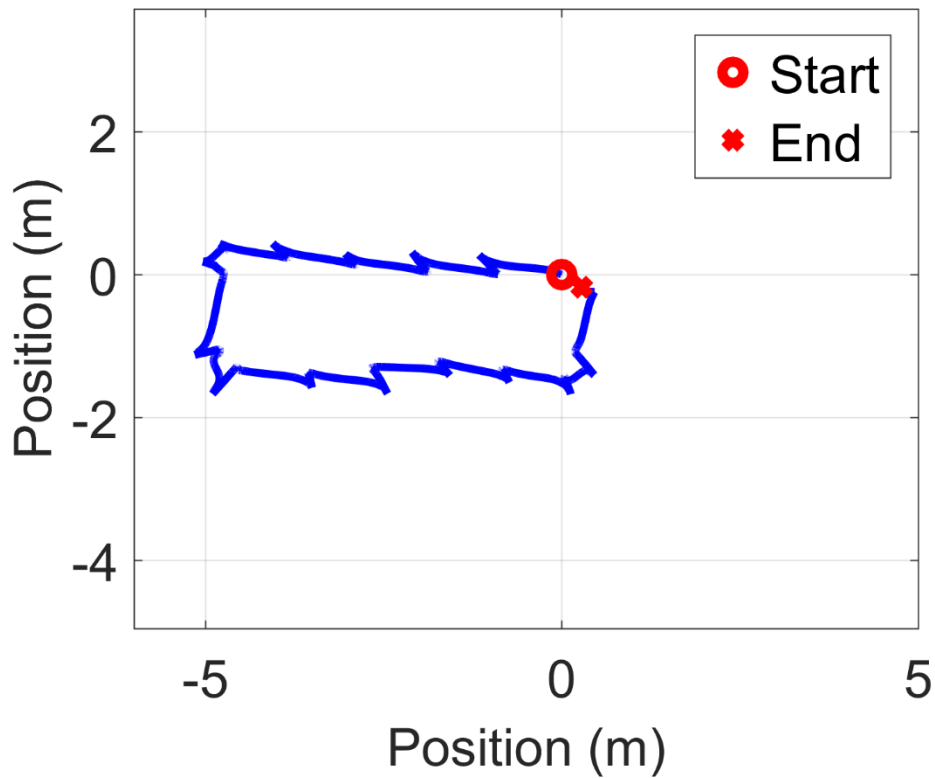


Figure 3. 7: Estimated walking path for 25 s based on the proposed ZUPT method.

### 3.3 Low-Pass Filter

After using the PDR system with the proposed ZUPT method to plot the path on map, we can get a more accurate result. From the map plot, however, we can see that the blue line representing the walking path is sharp. Different from the smooth line, the sharp walking path line reduces the acceptability of the appearance of the walking path and increases the difficulty of comparison to ground truth. Therefore, an additional filter needs to be used to correct the plot results so that the lines in the plot will become smoother.

Through the analysis of the data, the pedestrian will continuously switch between the stance phase and the swing phase while walking, and ZUPT ensures that each data can accurately correspond to the walking state of the pedestrian. During the ZUPT method's working time, sharp corrections exist due to the error-state corrections being applied at each stance phase. We need to add filters to reduce the impact of sharp correction on the path line.

A low-pass filter is an electronic filtering device that allows signals below the cut-off frequency to pass but signals higher than the cut-off frequency cannot pass. There are many different forms of the low-pass filter concept, including electronic circuits (such as hiss filters used in audio equipment), digital algorithms for smoothing data, acoustic barriers, image blurring, etc. Both tools provide a smooth form of signal by eliminating short-term fluctuations and retaining long-term development trends. The role of the low-pass filter in signal processing is equivalent to that of other fields, such as the moving average in the financial field. If we combine both low-pass filter and the moving average's working principles together, we will get a type of filter: moving average filter. The essence of moving average is a kind of low-pass filtering. Its purpose is to filter out high-frequency disturbances in the time series and to retain useful low-frequency trends. The moving average filter is used to directly calculate the average weight of the time series, so it is simple to use.

The principle of the moving average filter is that the moving average filter is based on statistical rules and regards continuous sampled data as a length fixed to  $N$ . After a new measurement, the first piece of data of the above values is removed. The remaining  $N-1$  pieces of data are moved forward in turn, the new sampled data is linked and inserted, arithmetic operations are performed on this variable, and the connected result is used as the result of this measurement.

After using the moving average filter on the 25 s walking test data, the following figure is obtained. As we can see from Figure 3.8, the blue line becomes very smooth, and the filter helps create a more natural-looking walking path.

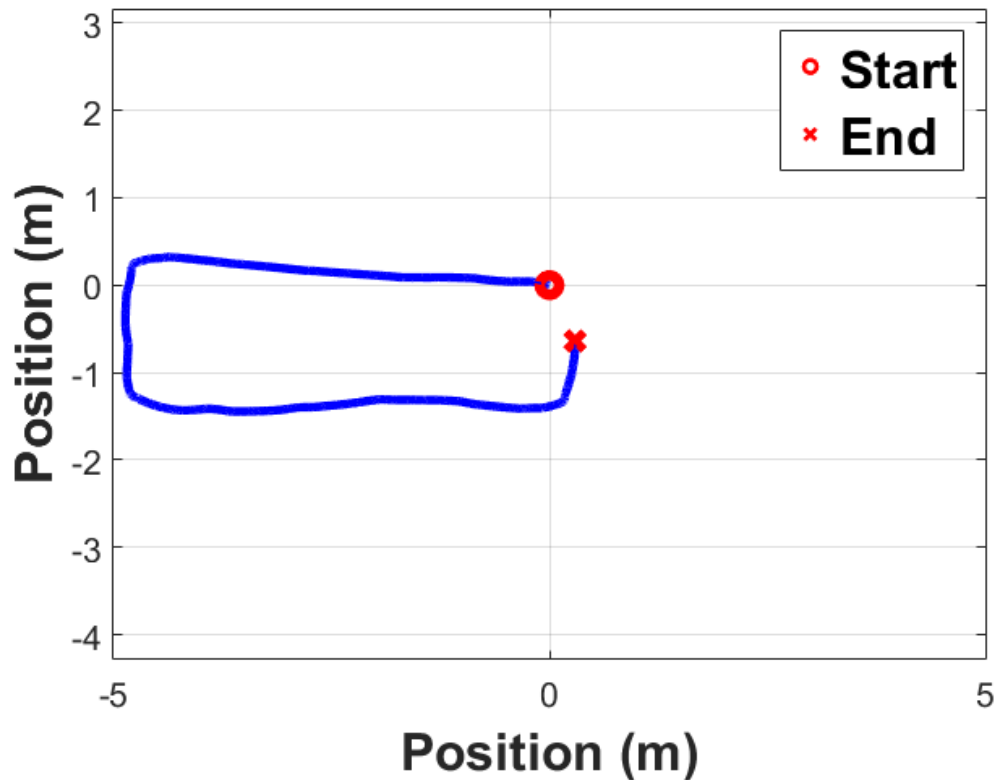
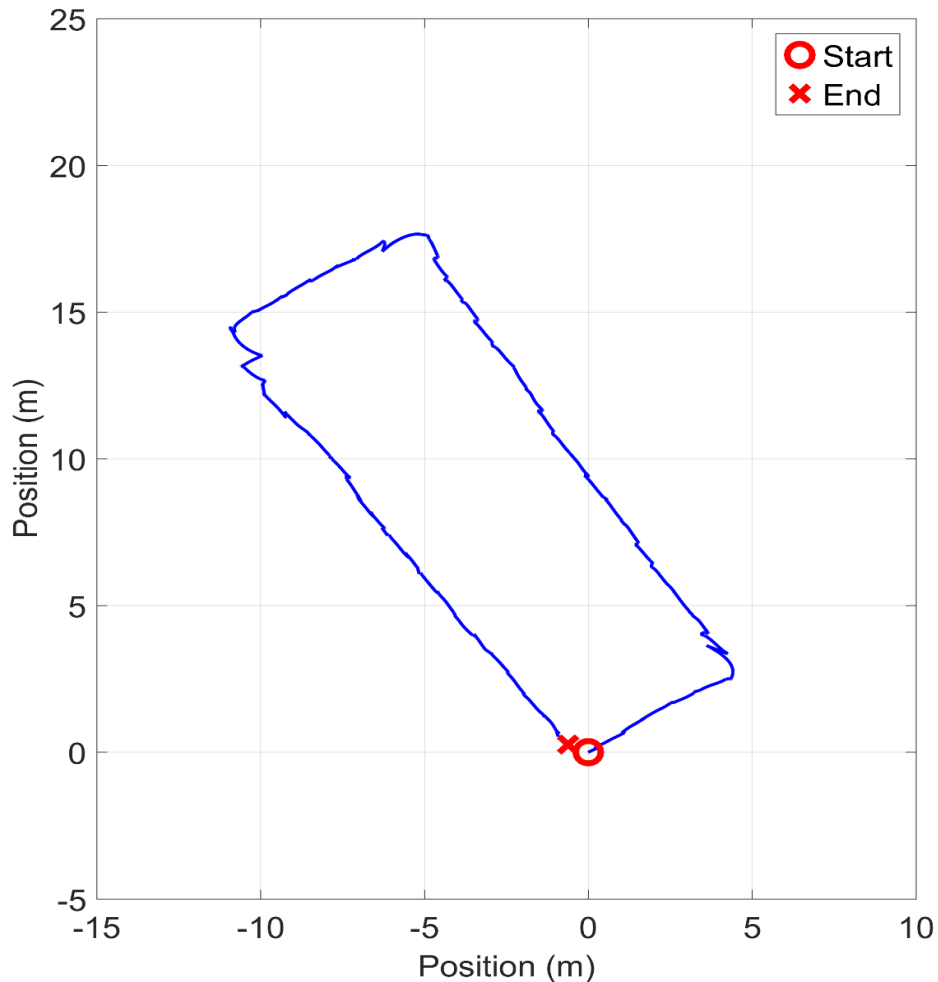


Figure 3. 8: Estimated walking path for 25 s based on the proposed ZUPT method with moving average filter.



In the moving average filter algorithm, the window size  $N$  is fixed to 200 to test if this window size  $N$  is suitable for long distance walking and will not cause the lag in data analysis process. Therefore, additional tests were performed in a rectangular indoor area of 5 m \* 20 m. Using the same algorithm to process the moving average filter of this set of data, the results are shown in Figure 3.9 and Figure 3.10. The estimated path line in Figure 3.10 has been smoothed by the moving average filter. The estimated path is basically the same as the actual walking path, so there is no hysteresis effect. Experiments have proved that, with the increase of walking data sets, the moving average filter can adapt to long-distance walking requirements without increasing the



**Figure 3. 9: Estimated walking path based on the proposed ZUPT method.**

window size  $N$ . Therefore,  $N = 200$  is suitable for long-distance tests.

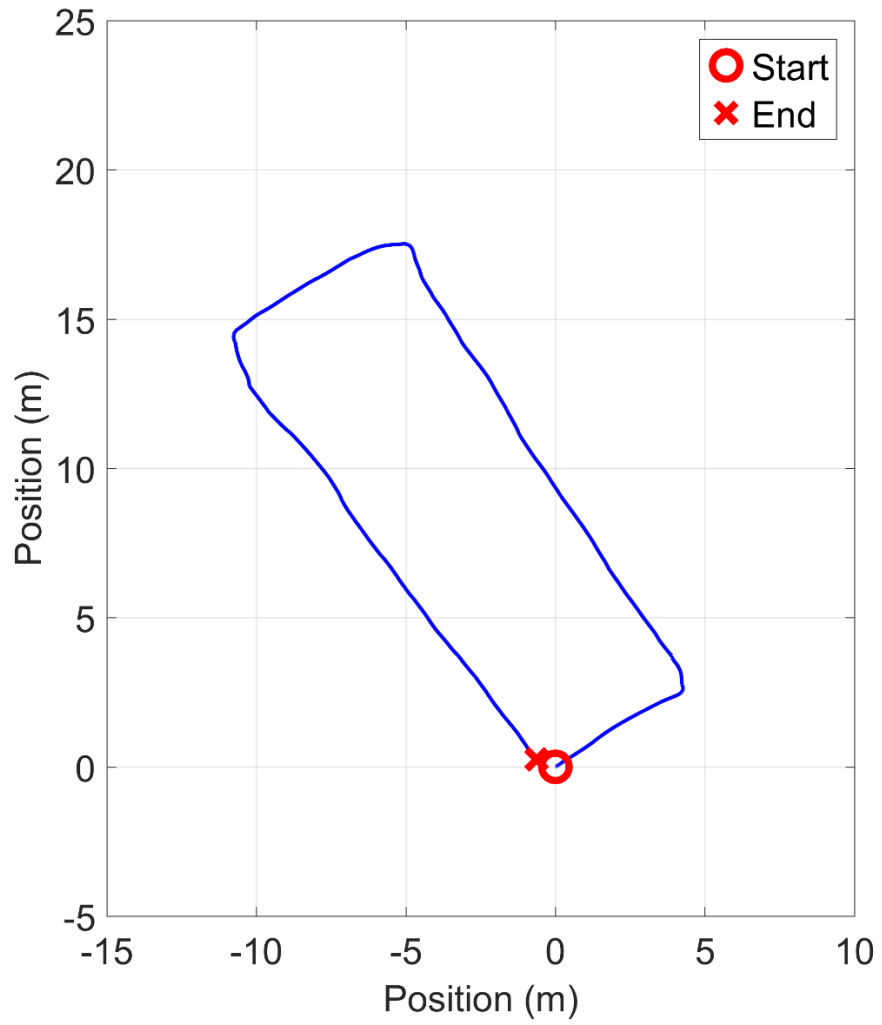


**Figure 3. 10: Estimated walking path based on the proposed ZUPT method with moving average filter.**

# Chapter 4: Results and Discussion

## 4.1 Step Detection

The most direct impact of ZUPT on PDR is detecting the number of steps pedestrians walk and the time interval between each step [56]. When the number of steps and the time are determined, the walk distance and speed of the pedestrian can be determined. Therefore, accurately detecting the number of steps taken by a pedestrian can better help to improve the PDR. By recording the actual number of steps in a certain walking period, the accuracy of the two ZUPT methods in calculating the number of steps can be found, as shown in Table XIV to Table XVII. In the different speed step detection experiments, the results of different re-detect threshold values were also compared. Three threshold values are selected based on the 100 Hz frequency of IMU sensor. These three threshold values are  $T_{data} = 10$ ,  $T_{data} = 20$ , and  $T_{data} = 5$ .

Table XIV shows the step detection results of walking speed at around 3-4 km/h. After one minute of walking, the single-threshold method can maintain an average accuracy of 72.36%, while the proposed ZUPT method at  $T_{data} = 10$  maintained an average accuracy above 92.12%. After five minutes of continuous walking results shown in Table XV, the average accuracy of the threshold method fell to 63.40%, while the proposed ZUPT method at  $T_{data} = 10$  could still maintain an average accuracy of 92.12%. For fast walking tests, the pedestrian walking speed was maintained at 4-6 km/h for 120 s. The step detection results are shown in Table XVI. After 120 s of walking, the single-threshold method can maintain an average accuracy of 61.21%, while our proposed ZUPT method at  $T_{data} = 10$  maintained an average accuracy above 85.50%. For the running test, the pedestrian running speed was maintained at 8-10 km/h for 120 s. The step detection results are shown in Table XVII. After 120 s of running, the single-threshold method could maintain an average accuracy of 37.97%, while our proposed ZUPT method at  $T_{data} = 10$  maintained an average accuracy above 79.86%.

The Table XIV, Table XV, and Table XVI show the results of method at  $T_{data} = 10$  and method at  $T_{data} = 20$  are almost the same in speed range 3-4 km/h and 4-6 km/h. Because in these two speed ranges, the pseudo intervals' size is generally less than 10, and the complete phase intervals' size is generally larger than 20. However, as the walking speed increases, the accuracy of step detection result at  $T_{data} = 20$  will decrease. In Table XVII, the proposed ZUPT method at  $T_{data} = 20$  only has 76.41% average accuracy which is less than the method at  $T_{data} = 10$ . This is because when the walking speed increase, the time to complete each step is reduced, and the corresponding data amount for completing a phase will also be reduced. The result is that a large threshold will replace the correct phase intervals with the wrong one. This will lead to error detection. When  $T_{data} = 5$ , there are more error detections than  $T_{data} = 10$  and  $T_{data} = 20$ , this is because  $T_{data} = 5$  cannot correctly distinguish the pseudo intervals with the size around 6-10, which leads to the missed detection of pseudo zero velocity intervals. This is the reason  $T_{data} = 5$  has the lowest average accuracy in these three re-detect threshold methods.

TABLE XIV					
Method	Test 1 Counted Steps	Test 2 Counted Steps	Test 3 Counted Steps	Test 4 Counted Steps	Average Accuracy
Real steps	40	43	42	40	—
Conventional ZUPT	28	31	27	33	72.36%
Proposed ZUPT (1) $T_{data} = 10$	36	38	41	37	92.12%
Proposed ZUPT (2) $T_{data} = 20$	36	38	40	37	91.53%
Proposed ZUPT (3) $T_{data} = 5$	34	36	37	37	87.33%

Table XIV: 60 s, 3-4 km/h Step Detection Results.

TABLE XV					
Method	Test 1 Counted Steps	Test 2 Counted Steps	Test 3 Counted Steps	Test 4 Counted Steps	Average Accuracy
Real steps	188	194	183	186	—
Conventional ZUPT	117	126	121	113	63.40%
Proposed ZUPT (1) $T_{data} = 10$	164	171	169	175	90.46%
Proposed ZUPT (2) $T_{data} = 20$	164	171	169	175	90.46%
Proposed ZUPT (3) $T_{data} = 5$	151	167	148	145	81.31%

Table XV: 300 s, 3-4km/h Step Detection Results.

TABLE XVI					
Method	Test 1 Counted Step	Test 2 Counted Step	Test 3 Counted Step	Test 4 Counted Step	Average Accuracy
Real steps	137	138	135	142	—
Conventional ZUPT	84	87	79	88	61.21%
Proposed ZUPT (1) $T_{data} = 10$	115	119	115	123	85.50%
Proposed ZUPT (2) $T_{data} = 20$	115	118	115	120	84.79%
Proposed ZUPT (3) $T_{data} = 5$	103	101	108	101	74.88%

Table XVI: 120s, 4-6 km/h Step Detection Results.

TABLE XVII					
Method	Test 1 Counted Step	Test 2 Counted Step	Test 3 Counted Step	Test 4 Counted Step	Accuracy
Real steps	269	251	266	273	—
Conventional ZUPT	98	102	107	94	37.97%
Proposed ZUPT (1) $T_{data} = 10$	208	211	209	217	79.86%
Proposed ZUPT (2) $T_{data} = 20$	203	206	202	197	76.41%
Proposed ZUPT (3) $T_{data} = 5$	174	168	171	156	63.26%

Table XVII: 120s, 8-10 km/h Step Detection Results.

Because the diversity of samples in step detection tests is limited, the data in this experiment can only show the experimental results of the samples participating in the experiment. In terms of the current testing sample size and the experimental results, step detection experiments have shown that the proposed ZUPT method can better maintain the accuracy of step detection during long-term pedestrian walking and running tests which plays a key role for PDR in judging pedestrian gait changes. Also, the step detection experiments shows that when the working frequency of the IMU is 100 Hz, the re-detect threshold value equal to 10 is suitable for all the walking speeding ranges.

## 4.2 Navigation Map Plot

We have tested the performance of the proposed ZUPT method when walking a short distance of 25 s in indoor environment, and the proposed ZUPT method has obtained good position tracking results. To test the stability of this method during long periods of walking, two test experiments have been designed.

The first experiment is a short-term multi-action experiment, with a testing time of 60 s, and the area of the experiment is a 5 m \* 4 m rectangle in indoor environment. In this experiment, pedestrians need to walk around the area within 60 s, and the walking involves multiple turning movements. The purpose is to test the stable performance of the proposed ZUPT method compared with the single-threshold ZUPT method. Figure 4.1 shows the performance of the conventional ZUPT method in this experiment. We can see from Figure 4.1 that, in the experiment with fast cadence, the error accumulation

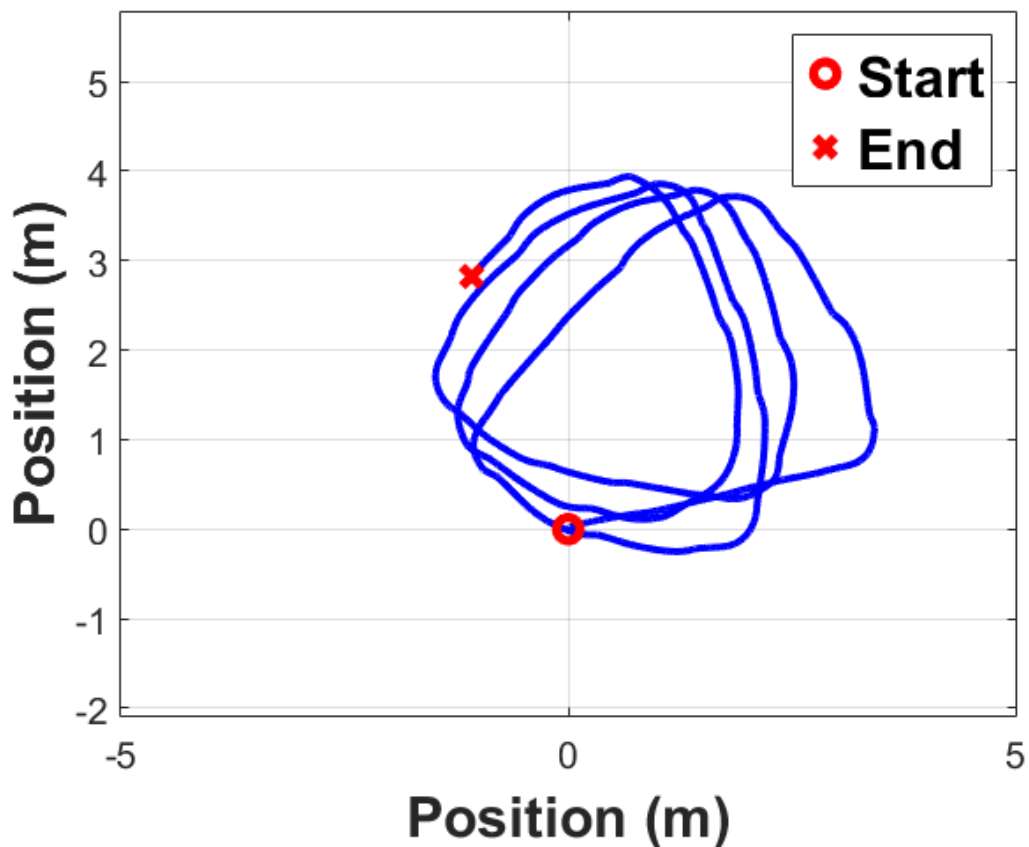


Figure 4. 1: Estimated walking path for 60 s based on single-threshold ZUPT method.

of the conventional ZUPT method is extremely fast, and the head drifting error has already occurred at the first turn. After many turns, the conventional method can no longer maintain the pedestrian path in the rectangular area shape.

Figure 4.2 shows the performance of the proposed ZUPT method. Because the proposed ZUPT method has more accurate phase judgment, this method is more accurate in the estimation of the pedestrian's path. In the Figure 4.2, this method better maintains the path of pedestrians and maintains the rectangular shape of the route, even after many turns.

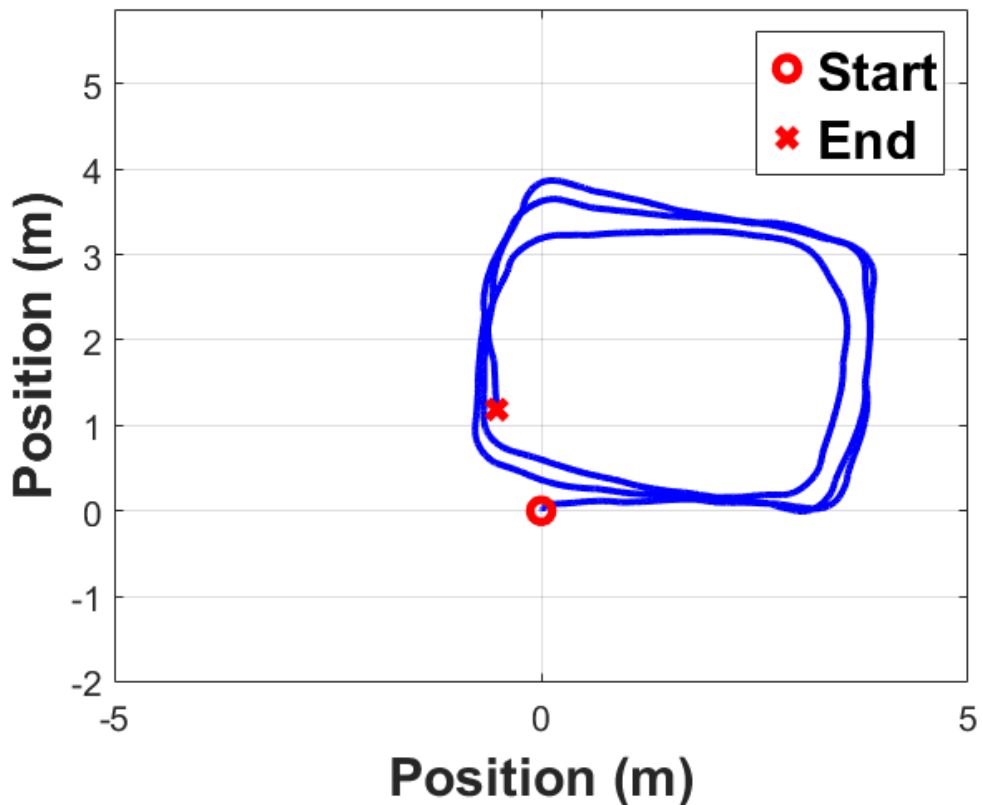


Figure 4. 2: Estimated walking path for 60 s based on proposed ZUPT method.

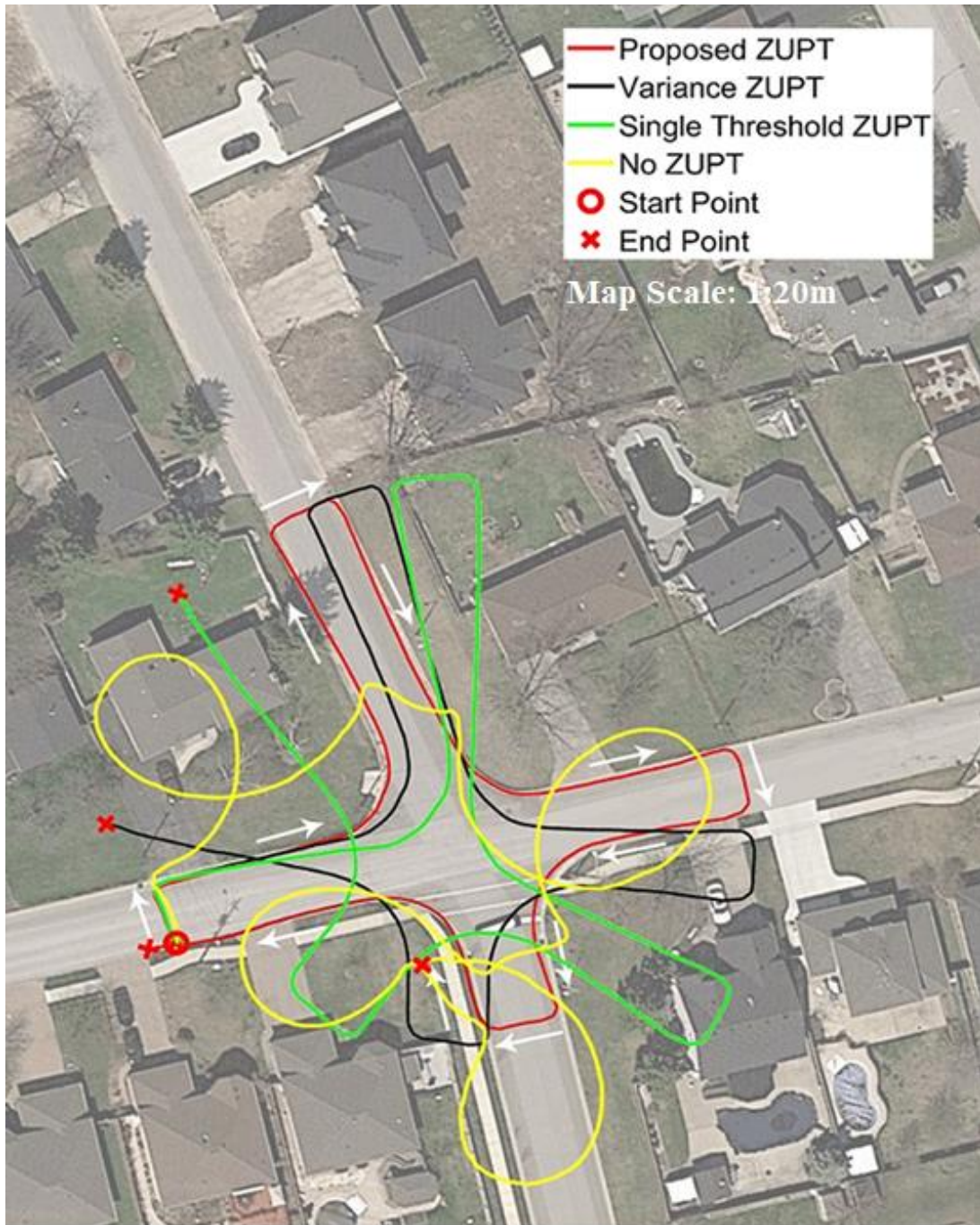
By comparing the proposed ZUPT method with conventional methods in an indoor environment, it is found that the proposed ZUPT method can better maintain the walking path shape and is not limited to the influence of indoor environmental factors. The result proves that in indoor environment, the proposed ZUPT method has better position tracking ability.

After proving that the proposed ZUPT method can maintain good tracking



performance in indoor environments, to test the performance of the proposed ZUPT method in a large area, an open outdoor environment will be selected as the test space for the next stage.

To analyze the performance difference between the proposed ZUPT method and the conventional ZUPT methods more intuitively, we selected a road intersection for a



Maps Data: Google, ©2020 First Base Solution, Maxar Technologies, Sanborn, U.S. Geological Survey, USDA Farm Service Agency

**Figure 4. 3: The 3-7 km/h walking test based on satellite map background.**

walking test location. The test will use a Google satellite map as the background for pedestrian walking path estimation. The map scale is 1:20m. The testing speed will be freely switched by the pedestrian between 3-7 km/h during the testing time, as shown in Figure 4.3. In this test, the total testing time is 610s, and the total number of actual walking steps is 408 steps. Different ZUPT methods will process the same set of walking data, output the result of step detection, and estimate the walking path on the satellite map.

The red line indicates the proposed ZUPT method, the black line indicates single-threshold-variance ZUPT method, the green line indicates single- threshold ZUPT method, and the yellow line indicates no ZUPT method. As can be seen from Figure 4.3, the proposed method can better adapt to the complex terrain of the intersection, including the four arc-shaped roadsides [57]. The white arrows show the pedestrian real walking direction during the test. For the no ZUPT method, which is shown by the yellow line, because of the lack of algorithms and filters to control errors, the heading drift error and the walking path error are out of control, this method performed the worst in this test. For the single-threshold method shown by the green line, the detection of the pedestrian walking phase is not accurate due to the limitation of the single threshold, and the position drift error appears very early in this speed switching test. Therefore, the single-threshold method performed very badly in this test. The variance method benefits from the variance algorithm's ability to maintain data stability, and the performance in this test is better than the single-threshold method which is shown by the black line in Figure 4.3.

The Table XVIII shows the step detection results for this test. The proposed ZUPT method has 92.15% accuracy compared with the actual counted step numbers. The variance ZUPT method has 79.17% and the single threshold ZUPT method has only 62.25%.

TABLE XVIII		
Method	Counted Step	Accuracy
Real steps	408	—
Proposed ZUPT	376	92.15%
Variance ZUPT	323	79.17%
Single Threshold ZUPT	254	62.25%
<b>Total Testing Time</b>	610 s	
<b>Sensor Accelerometer Bias</b>	0.00383 $m/s^2$	
<b>Sensor Gyroscope Bias</b>	-0.0072 $rad/s$	
<b>Map Scale</b>	1:20 m	

**Table XVIII: The step detection results in satellite map test.**

The results of the test show that in the case of processing a same set of pedestrian walking data, the proposed ZUPT method has the best performance in this test and can better maintain the estimated shape of the pedestrian walking path when switching between different speeds under different road conditions.

Then, to test the performance of the method in the long-time walking test, a more open area was selected for the next experiment. The purpose of this experiment is to test whether the proposed ZUPT method can maintain the accuracy of step detection in long-time experiments, and whether it can completely estimate the walking path of pedestrians on satellite maps.

Figure 4.4 shows the results of the walking test at a speed of 3-4km/h for 35

minutes and 28 seconds by using the proposed ZUPT method. The map scale is 1:20 m. The experiment has walked a total of two laps. The first lap is marked with a red line in Figure 4.4. The duration of this lap is 16 minutes and 8 seconds. The second lap is marked with a blue line in Figure 4.4, and the duration of this lap is 19 minutes and 20 seconds. In the first lap of walking, to avoid vehicles and other pedestrians, there are three obvious avoidance behaviors, which shown in the figures. The avoidance behavior was also recorded and fully reflected on the map results, which also showed that this proposed method has practical application capabilities.

Table XIX shows the testing data of the IMU sensor and the step detection results for proposed ZUPT method, variance ZUPT method and single threshold ZUPT method. From Table XIX, the proposed ZUPT method can still maintain 90.41% accuracy in the whole walking test, which help PDR to better detect the walking gait and eliminate errors. Compared with the other two conventional methods, the proposed ZUPT method maintains better accuracy and maintains the same level as in previous shorter distance testing. And on the satellite map, the PDR which using the proposed ZUPT method can completely track the positioning information of pedestrians.



Maps Data: Google, ©2020 First Base Solution, Maxar Technologies, Sanborn, U.S. Geological Survey, USDA Farm Service Agency

**Figure 4. 4: 3-4 km/h long-time walking test**

<b>TABLE XIX</b>		
<b>Method</b>	<b>Counted Step</b>	<b>Accuracy</b>
Real steps	1836	—
Proposed ZUPT	1660	90.41%
Variance ZUPT	1531	83.39%
Single Threshold ZUPT	1097	59.75%
<b>Total Testing Time</b>	35min 28 s	
<b>First Lab Time</b>	16 min 8 s	
<b>Second Lab Time</b>	19 min 20 s	
<b>Total Distance</b>	2.36 km	
<b>Sensor Accelerometer Bias</b>	0.00219 $m/s^2$	
<b>Sensor Gyroscope Bias</b>	-0.00343 $rad/s$	
<b>Map Scale</b>	1:20 m	

**Table XIX: 3-4km/h long-time walking test.**

### 4.3 Eight-Point Error Method

The eight-point error method is used to calculate the error between the estimated data and the real data [25]. Eight actual measured ground truth points are set in a specified area as reference coordinates, marked in the simulation area plot. Then, the pedestrian carries the device and does the walking experiment in the specified area, along the designated route. Through the collection and processing of walking data, the pedestrian's walking path is estimated, and, then, the estimated coordinates of the pedestrian's location when passing these eight measured points are marked. The coordinates of the eight estimated points are compared to the coordinates of the eight measured points, then the error values are calculated on both X-axis and Y-axis. In this thesis, a rectangular space of about 30 m \* 20 m was selected for the error experiment.

As shown in Figure 4.5 and Figure 4.6, the eight red star marks are the measured coordinate points, and the eight green star marks are the estimated coordinate points.

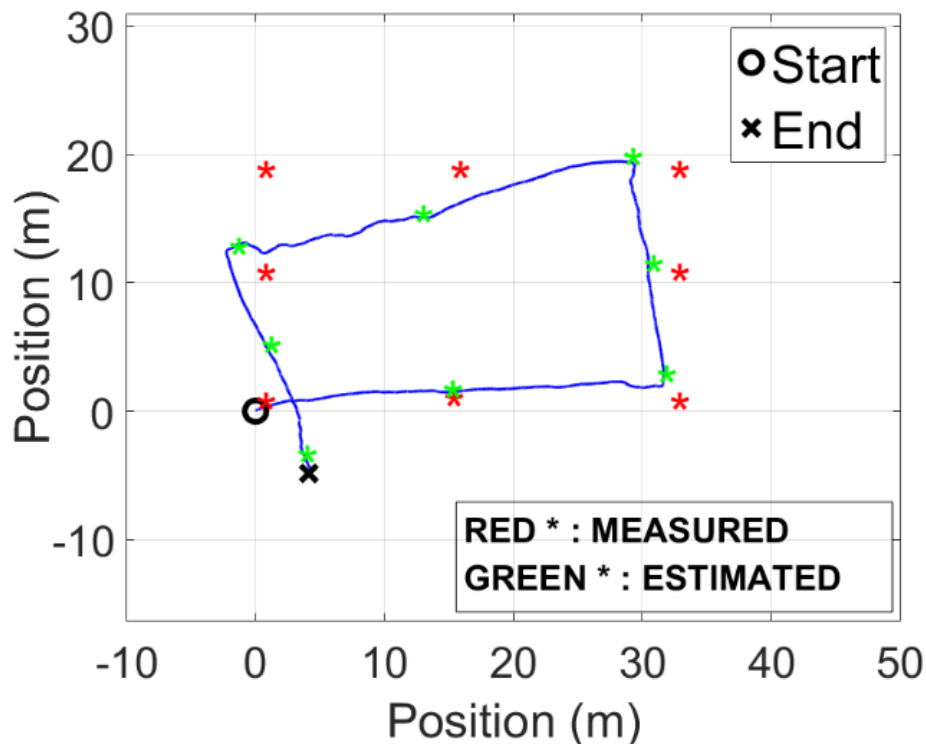


Figure 4. 5: Eight-point error method for single-threshold ZUPT method.

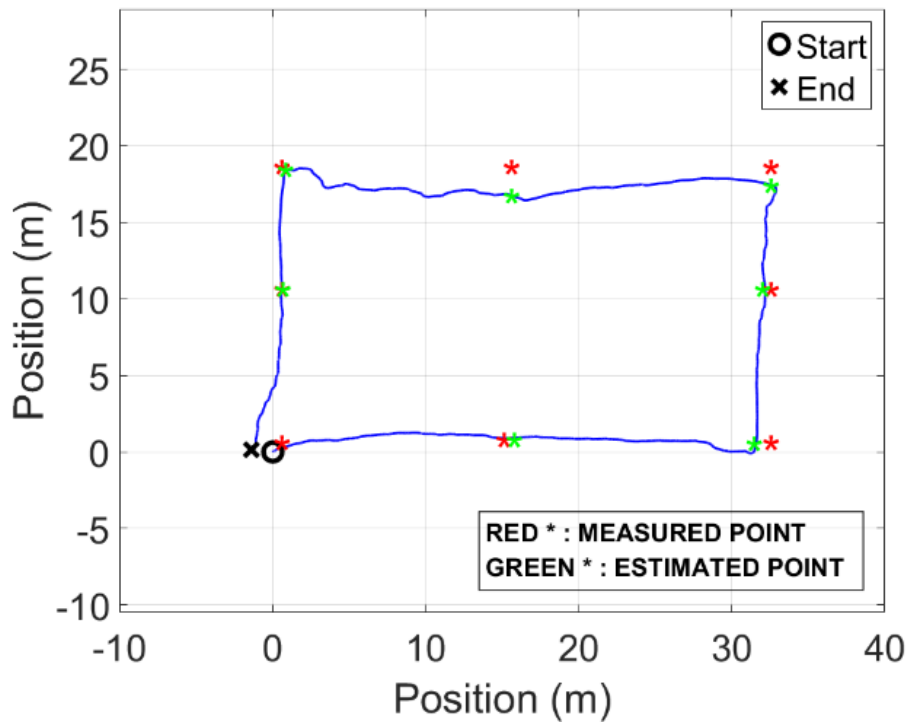


Figure 4. 6: Eight-point error method for the proposed ZUPT method.

Due to the different ZUPT methods, the drift error of eight points is also different. Table XX shows all the eight coordinate points for the two methods, calculates the mean error, and compares them with each other.

By analyzing the path map of the conventional, single-threshold ZUPT method and comparing the eight estimated coordinates with the actual eight measured ground truth coordinates, the error value of the eight points in the path map is obtained, which is represented by a line chart, shown in Figure 4.7. In the conventional ZUPT method error plot, the mean error is 3.33 m, and the peak error is 6.36 m.

By analyzing the path map of the proposed ZUPT method and comparing the eight estimated coordinates with the actual eight measured ground truth coordinates, the error value of the eight points in the path map is obtained; the error value is represented by a line chart shown in Figure 4.8. In the proposed ZUPT method error plot, the mean error

is 0.61 m, and the peak error is 1.18 m, a reduction of 81.69% and 81.44%, respectively.

<b>TABLE XX</b>				
<b>Ground Truth Points</b>	<b>Proposed ZUPT</b>	<b>Error (m)</b>	<b>Conventional ZUPT</b>	<b>Error (m)</b>
(0,0)/(0,0)	(0,0)/(-0.13,0.13)	0.130	(0,0)/(4.07, -4.19)	5.839
(15,0)	(15.2,0.88)	0.904	(14.44,1.49)	1.594
(32,0)	(31.4, -0.06)	0.592	(31.57,2.05)	2.096
(32,10)	(32.2,10)	0.200	(30.45,10.68)	1.693
(32,18)	(32.9,17.28)	1.152	(29.25,19.34)	3.059
(15,18)	(15,16.82)	1.180	(12.66,15.08)	3.742
(0,18)	(0.79,18.26)	0.772	(-2.18,12.03)	6.357
(0,10)	(0.55,10)	0.550	(1.09,4.55)	5.558
<b>Mean of Total Error (m)</b>	<b>0.609</b>		<b>3.326</b>	
<b>Percentage</b>	<b>0.609%</b>		<b>3.326%</b>	

**Table XX: Eight-point coordinates comparison.**



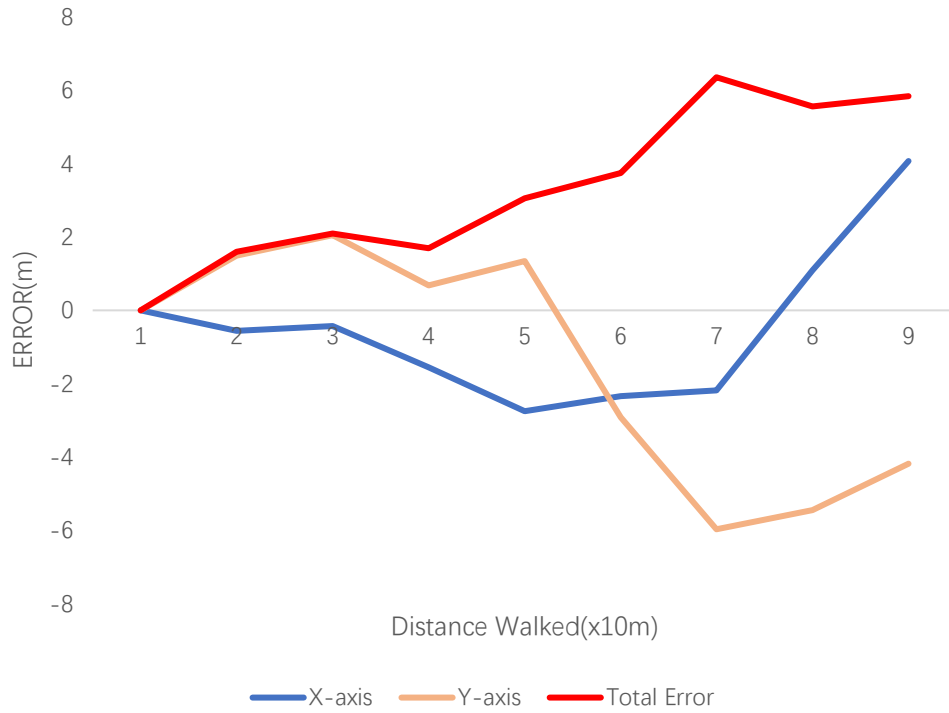


**Figure 4. 7: Error line graph for the conventional ZUPT method.**



**Figure 4. 8: Error line graph for the proposed ZUPT method.**

Table XX shows the experimental results comparison between the proposed ZUPT method-based PDR system and other PDR systems which introduced before. The Table XXI shows that compared with other systems, the proposed method has better error control ability in walking experiments, and the error range is smaller than most PDR system results.

Therefore, the proposed ZUPT method-based PDR system achieves the goal of improving the positioning accuracy by re-detect and correct the pseudo zero velocity intervals. It has a significant effect of error control without additional equipment assistance, showing comparable accuracy achieved with the proposed PDR system.

<b>TABLE XXI</b>			
<b>Method</b>	<b>Experiment</b>	<b>Error</b>	<b>Percentage</b>
Quaternion vector-based PDR	380 m walking route	2.57 m	0.68%
Waist-mounted PDR	64.48 m walking route	1.934 m	2.99%
Dual-mounted PDR (foot- and leg-mounted)	23 m walking route	0.286 m	1.24%
Ultrasonic sensor foot-mounted PDR	120 m walking route	0.53 m	0.44%
The proposed ZUPT method-based PDR	100 m walking route	0.609 m	0.609%

**Table XXI: Comparison between different PDR methods.**

# Chapter 5: Summary and Conclusions

## 5.1 Summary

Nowadays, since the pedestrian inertial navigation system has a real-time autonomous navigation function and does not require external information such as satellite signals, it occupies a place in personal information navigation systems. More precise positioning functions and error correction functions, as well as higher reliability and flexibility, have always been the characteristics pursued by pedestrian inertial navigation systems. These are also the goals which are pursued in this thesis. By studying the conventional ZUPT methods in the pedestrian dead reckoning system and proposing a new ZUPT method, the positioning accuracy of the pedestrian dead reckoning system is improved, which brings more possibilities for applications of the pedestrian dead reckoning in the future.

Within this thesis is the definition, and validation of such a method that based on not adding additional sensors, the proposed ZUPT method is used to perform secondary detection and correction of the pseudo zero velocity intervals in the PDR system to strengthen the ability to track the walking phase of pedestrians, improve the accuracy of step detection, and achieve the purpose of controlling drift errors.

Among the work completed at the current stage, step detection experiments have been completed under different speeds and different time range conditions, and for different re-detect threshold values, the experimental data are also compared. For 3-6 km/h walking speed step detection tests, the accuracy of the proposed ZUPT method has an average 23.7% higher than the conventional methods. In a long-distance walking path tracking test, the mean error of the estimated path for our method is 0.61 m, which is an 81.69% reduction compared to the conventional ZUPT methods. The proposed ZUPT method performed well in these experiments. In addition, in the satellite map walking experiment, this method also estimated the same walking trajectory as the

actual walking path. The proposed ZUPT method has certain potential in the field of pedestrian inertial navigation and can be applied to further navigation projects. It can replace the conventional ZUPT methods.

## **5.2 Future Work**

To advance the work outlined in this thesis, further investigation into other uses of the proposed ZUPT method is recommended. The current experiments are based on the 2D coordinate system. In reality, if want to make more accurate estimation for pedestrians' walking phases and path, the calculations in the 3D coordinate system must be developed. In this thesis, the thresholds of all motion states have been summarized, including jumping, climbing stairs, etc., and these thresholds can help complete the construction of the pedestrian state in the 3D coordinate system. Moreover, due to the limitations of the threshold test at this stage, the base number of the sample size is small, which may cause the threshold to be unable to adapt to more people after the expansion of the method. In future work, the extension of the threshold sample size required in the method will be of great help to the generalization of this method. For the re-detect threshold, increasing the size of the test sample at 100 Hz will help narrow the range of the re-detect threshold and better analyze the work efficiency of different re-detect thresholds under different walking test conditions, such as different walking speeds.

In addition to the method of expanding the sample size and calculate more accuracy threshold ranges, there are other methods that can help the proposed method to better expand the scope of application. The machine learning method could be another way of helping the threshold adapt to the pedestrian who has a highly unusual gait patterns [58]. Machine learning would allow the system to glean insight into the user's gait, and adapt accordingly, reduce unnecessary errors, and increase the population size of the individuals who can use this device for navigation purposes.

The proposed method has a small-volume algorithm structure, which can be expanded in the future, such as by adding more targeted filters to achieve the purpose of improving accuracy or combining with other sensors to improve the tracking ability of pedestrian trajectories. This method has better compatibility than traditional ZUPT methods.

The development of GNSS has greatly matured in modern times. GNSS has always been in a leading position in positioning services. Pedestrian inertial navigation systems do not exist to seize the market with GNSS but can be combined with a GNSS system to complement each other. In future work, we can combine the proposed ZUPT method-based PDR system with GNSS system to further expand the application range of pedestrian inertial navigation systems.

### **5.3 Conclusions**

This thesis provides a new type of ZUPT method to help the shoe-mounted PDR system to locate and navigate pedestrians. Analyze the gait data of pedestrians collected by IMU through the conventional PDR system, and summarize the data changes during pedestrian walking, the new ZUPT method was proposed that uses information collected from these data. Under the premise of not adding additional sensors, this method improves the gait tracking ability of pedestrians during walking by adding the re-detect algorithm for correcting pseudo zero velocity intervals, controls the drift error, and meets the requirements of improving pedestrian positioning accuracy. This method provides a foundation for the future design and programming of pedestrian inertial navigation system augmentation using low-cost IMU device. This method shows strong potential for indoor pedestrian navigation systems augmentation providing the basis for future services and applications where an accurate user location is required.

## REFERENCE AND BIBLIOGRAPHY

- [1] G. Zheng, W. Qiuying and Z. Minghui, "Research on indoor pedestrian location based on miniature inertial measurement unit," *2017 Forum on Cooperative Positioning and Service (CPGPS)* , Harbin, 2017, pp. 289-293, doi: 10.1109/CPGPS.2017.8075141.
- [2] P. D. Groves, "Principles of GNSS, inertial, and multisensor integrated navigation systems, 2nd edition [Book review]," in *IEEE Aerospace and Electronic Systems Magazine*, vol. 30, no. 2, pp. 26-27, Feb. 2015.
- [3] V. Vasile, C. Naornita and M. Borda, "Comparative Study of Satellite Navigation Systems," *2018 International Symposium on Electronics and Telecommunications (ISETC)*, Timisoara, 2018, pp. 1-6.
- [4] F. Hui and F. Qin, "Influence of Inertial Sensor Errors on GNSS/INS Integrated Navigation Performance," *2016 Eighth International Conference on Measuring Technology and Mechatronics Automation (ICMTMA)*, Macau, 2016, pp. 347-351.
- [5] L. X. Zheng, W. C. Zhou, W. W. Tang, X. C. Zheng, A. Peng, H. R. Zheng, "A 3D indoor positioning system based on low cost MEMS sensors," *Simulation Modelling Practice and Theory* ,2016, pp. 45–56.
- [6] E. Au, "Feature Updates for Wi-Fi Alliance [Standards]," in *IEEE Vehicular Technology Magazine*, vol. 11, no. 4, pp. 15-16, Dec. 2016.
- [7] A. Correa, M. Barcelo, A. Morell, J. L. Vicario, "A review of pedestrian indoor positioning systems for mass market applications," *Sensors*, vol. 17, 2017.
- [8] "Gyroscopes and IMUs for Defense, Aerospace & Industrial," Yole Developpement, 2012. [Online]. Available: [http://www.yole.fr/iso\\_upload/Yole\\_Gyro\\_MU\\_Report\\_Sample\\_September\\_2012.p df](http://www.yole.fr/iso_upload/Yole_Gyro_MU_Report_Sample_September_2012.pdf). [Accessed: 29-Apr-2019].
- [9] P. S. Marinushkin and I. A. Podshivalov, "MEMS-based non-orthogonal redundant inertial measurement unit for miniature navigation systems," *2015 International*

*Siberian Conference on Control and Communications (SIBCON)*, Omsk, 2015, pp. 1-3.

[10] A. Perttula, J. Parviainen and J. Collin, "Pedestrian detection with high resolution inertial measurement unit," *2016 IEEE SENSORS*, Orlando, FL, 2016, pp. 1-3.

[11] Y. N. Korkishko *et al.*, "High-precision inertial measurement unit IMU-5000," *2018 IEEE International Symposium on Inertial Sensors and Systems (INERTIAL)*, Moltrasio, 2018, pp. 1-4.

[12] D. Lemmerhirt *et al.*, "Improved Scale-Factor and Bias Stability of Ovenized Inertial Sensors in an Environmentally-Stabilized Inertial Measurement Unit (eIMU)," *2019 IEEE International Symposium on Inertial Sensors and Systems (INERTIAL)*, Naples, FL, USA, 2019, pp. 1-4.

[13] X. Hou and J. Bergmann, "Pedestrian Dead Reckoning With Wearable Sensors: A Systematic Review," in *IEEE Sensors Journal*, vol. 21, no. 1, pp. 143-152, 1 Jan.1, 2021, doi: 10.1109/JSEN.2020.3014955.

[14] G. Wang, X. Wang, J. Nie and L. Lin, "Magnetic-Based Indoor Localization Using Smartphone via a Fusion Algorithm," in *IEEE Sensors Journal*, vol. 19, no. 15, pp. 6477-6485, 1 Aug.1, 2019, doi: 10.1109/JSEN.2019.2909195.

[15] O. V. Altinpinar and M. E. Yalçın, "Design of a pedestrian dead-reckoning system and comparison of methods on the system," *2018 26th Signal Processing and Communications Applications Conference (SIU)*, Izmir, 2018, pp. 1-4.

[16] Y. Sakuma and M. Fujii, "A Study on Direction Estimation of Movement by Multiple Sensors for Pedestrian Dead-Reckoning," *2017 Fifth International Symposium on Computing and Networking (CANDAR)*, Aomori, 2017, pp. 603-605.

[17] I. A. Nagin and Y. M. Inchagov, "Effective integration algorithm for pedestrian dead reckoning," *2018 Moscow Workshop on Electronic and Networking Technologies (MWENT)*, Moscow, 2018, pp. 1-4.

[18] A. Ali, H-W. Chang, J. Georgy, Z. Syed, C. Goodall, "Heading Misalignment Estimation between Portable Devices and Pedestrians", *ION GNSS*, pp. 1626-1634, 2013.

[19] D. H. Titterton, *Strapdown inertial navigation technology*, 2nd ed. Stevenage, UK ;

Reston, VA: Institution of Electrical Engineers, 2004.

[20] Z. Fu, G. Zhang, Y. Lin, Y. Liu and J. Tan, "Calibration and compensation of inertial sensor errors in portable applications — a review," *2016 UKACC 11th International Conference on Control (CONTROL)*, Belfast, 2016, pp. 1-4.

[21] R. P. Suresh, V. Sridhar, J. Pramod and V. Talasila, "Zero Velocity Potential Update (ZUPT) as a Correction Technique," *2018 3rd International Conference On Internet of Things: Smart Innovation and Usages (IoT-SIU)*, Bhimtal, 2018, pp. 1-8.

[22] S. K. Park, Y. S. Suh, H. J. Kang and Y. S. Ro, "Zero velocity detection for inertial sensor-based personal navigation systems," *Proceedings of SICE Annual Conference 2010*, Taipei, 2010, pp. 1755-1758.

[23] I. Skog, P. Handel, J. Nilsson and J. Rantakokko, "Zero-Velocity Detection—An Algorithm Evaluation," in *IEEE Transactions on Biomedical Engineering*, vol. 57, no. 11, pp. 2657-2666, Nov. 2010.

[24] J. Wahlström, I. Skog, F. Gustafsson, A. Markham and N. Trigoni, "Zero-Velocity Detection—A Bayesian Approach to Adaptive Thresholding," in *IEEE Sensors Letters*, vol. 3, no. 6, pp. 1-4, June 2019, Art no. 7000704.

[25] M. Straeten and M. J. Ahamed, "Intuitive ultrasonic INS augmentation for pedestrian path tracking and navigation," in *Sensors and Actuators A: Physical*, vol. 299, no. 111641, Nov. 2019.

[26] W. Fan and Y. Li, "Accuracy analysis of sigma-point Kalman filters," *2009 Chinese Control and Decision Conference*, Guilin, 2009, pp. 2883-2888.

[27] X. Tong *et al.*, "A Double-Step Unscented Kalman Filter and HMM-Based Zero-Velocity Update for Pedestrian Dead Reckoning Using MEMS Sensors," in *IEEE Transactions on Industrial Electronics*, vol. 67, no. 1, pp. 581-591, Jan. 2020.

[28] J. Wahlström and I. Skog, "Fifteen Years of Progress at Zero Velocity: A Review," in *IEEE Sensors Journal*, vol. 21, no. 2, pp. 1139-1151, 15 Jan. 2021, doi: 10.1109/JSEN.2020.3018880.

[29] E. Munoz Diaz, S. Kaiser, and D. Bousdar Ahmed, "Height Error Correction for Shoe-Mounted Inertial Sensors Exploiting Foot Dynamics.," *Sensors (Basel, Switzerland)*, vol. 18, no. 3, 2018.



- [30] R. P. Suresh, V. Sridhar, J. Pramod and V. Talasila, "Zero Velocity Potential Update (ZUPT) as a Correction Technique," *2018 3rd International Conference On Internet of Things: Smart Innovation and Usages (IoT-SIU)*, Bhimtal, 2018, pp. 1-8.
- [31] H. Liu *et al.*, "An adaptive selection algorithm of threshold value in zero velocity updating for personal navigation system," *Proceedings of the 33rd Chinese Control Conference*, Nanjing, 2014, pp. 1035-1038.
- [32] Y. Ben, G. Yin, W. Gao and F. Sun, "Improved filter estimation method applied in zero velocity update for SINS," *2009 International Conference on Mechatronics and Automation*, Changchun, 2009, pp. 3375-3380.
- [33] R. Zhang, H. Yang, F. Höflinger and L. M. Reindl, "Adaptive Zero Velocity Update Based on Velocity Classification for Pedestrian Tracking," in *IEEE Sensors Journal*, vol. 17, no. 7, pp. 2137-2145, 1 April, 2017.
- [34] A. Jiménez *et al.*, "Indoor Pedestrian Navigation Using an INS/EKF Framework for Yaw Drift Reduction and a Foot-Mounted IMU," Proc. of Workshop on Positioning, Navigation and Communication (WPNC 10), IEEE, 2001, pp. 135–143.
- [35] G.A. Campbell, "On loaded lines in telephonic transmission," *The London, Edinburgh, and Dublin Philosophical Magazine and Journal of Science*, Series 6, Vol. 5(27):313-330, March 1903.
- [36] G.A. Campbell, "Electric wave-filter," U.S. Patent 1,227,113, July 15, 1915.
- [37] O.J. Zobel, "Theory and design of uniform and composite electric wave-filters," *The Bell System Technical Journal*, 2(1):1-46, January 1923.
- [38] S. Darlington, "Synthesis of reactance 4-poles which produce prescribed insertion loss characteristics," *Journal of Mathematics and Physics*, 18:257-353, 1939.
- [39] R. E. Kálmán, "A New Approach to Linear Filtering and Prediction," 1960.
- [40] Welch, G., & Bishop, G. (2001). Course 8 - An Introduction to the Kalman Filter. In *An Introduction to the Kalman Filter* (p. 5). Los Angeles, CA: SIGGRAPH.
- [41] M. Vemula, M. F. Bugallo and P. M. Djuric, "Performance Comparison of Gaussian-Based Filters Using Information Measures," in *IEEE Signal Processing Letters*, vol. 14, no. 12, pp. 1020-1023, Dec. 2007, doi: 10.1109/LSP.2007.906214.
- [42] "Multiple Model Adaptive Complementary Filter for Attitude Estimation,"

Aerospace Science and Technology, vol. 69, pp. 574–581, Oct. 2017.

[43] M. K. Mohd Salleh, "Out-of-band improvement of the quarter wavelength side-coupled ring resonator using low-pass filter integration," *2011 IEEE International Conference on System Engineering and Technology*, Shah Alam, Malaysia, 2011, pp. 128-131, doi: 10.1109/ICSEngT.2011.5993435.

[44] A. Coza and D. Jurisic, "Low-Noise and Low-Sensitivity Coupled Fourth-Order Low-Pass Filters," 2019 42nd International Convention on Information and Communication Technology, Electronics and Microelectronics (MIPRO), Opatija, Croatia, 2019, pp. 128-132, doi: 10.23919/MIPRO.2019.8756934.

[45] A. M. Sabatini, C. Martelloni, S. Scapellato and F. Cavallo, "Assessment of walking features from foot inertial sensing," in *IEEE Transactions on Biomedical Engineering*, vol. 52, no. 3, pp. 486-494, March 2005.

[46] Y. Wu, H. Zhu, Q. Du and S. Tang, "A Pedestrian Dead-Reckoning System for Walking and Marking Time Mixed Movement Using an SHSs Scheme and a Foot-Mounted IMU," in *IEEE Sensors Journal*, vol. 19, no. 5, pp. 1661-1671, 1 March 2019, doi: 10.1109/JSEN.2018.2884834.

[47] H. Ju, J. H. Lee and C. G. Park, "Pedestrian Dead Reckoning System Using Dual IMU to Consider Heel Strike Impact," *2018 18th International Conference on Control, Automation and Systems (ICCAS)*, Daegwallyeong, 2018, pp. 1307-1309.

[48] Jaehyun Park, Yunki Kim and Jangmyung Lee, "Waist mounted Pedestrian Dead-Reckoning system," *2012 9th International Conference on Ubiquitous Robots and Ambient Intelligence (URAI)*, Daejeon, 2012, pp. 335-336, doi: 10.1109/URAI.2012.6463008.


[49] N. Yu, Y. Li, X. Ma, Y. Wu and R. Feng, "Comparison of Pedestrian Tracking Methods Based on Foot- and Waist-Mounted Inertial Sensors and Handheld Smartphones," in *IEEE Sensors Journal*, vol. 19, no. 18, pp. 8160-8173, 15 Sept. 2019, doi: 10.1109/JSEN.2019.2919721.

[50] G. Eşsiz and G. Soysal, "Quaternion Vector Based Pedestrian Dead-Reckoning with Smartphones," *2019 27th Signal Processing and Communications Applications Conference (SIU)*, Sivas, Turkey, 2019, pp. 1-4, doi: 10.1109/SIU.2019.8806544.

- [51] S. K. Park and Y. S. Suh, "A Zero Velocity Detection Algorithm Using Inertial Sensors for Pedestrian Navigation Systems," *Sensors*, vol. 10, no. 10, pp. 9163–9178, Oct. 2010.
- [52] J. A. García-Molina et al., "Land mobile multipath channel reduction effects on a real GNSS receiver," 2010 5th ESA Workshop on Satellite Navigation Technologies and European Workshop on GNSS Signals and Signal Processing (NAVITEC), Noordwijk, Netherlands, 2010, pp. 1-7, doi: 10.1109/NAVITEC.2010.5708072.
- [53] N. El-Sheimy, H. Hou, and X. Niu, "Analysis and Modeling of Inertial Sensors Using Allan Variance," *IEEE Transactions on Instrumentation and Measurement*, vol. 57, no. 1, pp. 140–149, Jan. 2008.
- [54] Stančin, S., & Tomažič, S. š. (2014). Time- and Computation-Efficient Calibration of MEMS 3D Accelerometers and Gyroscopes. *Sensors*, 14(8), 14885–14915. <https://doi.org/10.3390/s140814885>
- [55] Y. Wang and A. M. Shkel, "Adaptive Threshold for Zero-Velocity Detector in ZUPT-Aided Pedestrian Inertial Navigation," in *IEEE Sensors Letters*, vol. 3, no. 11, pp. 1-4, Nov. 2019
- [56] A. Norrdine, Z. Kasmi and J. Blankenbach, "Step Detection for ZUPT-Aided Inertial Pedestrian Navigation System Using Foot-Mounted Permanent Magnet," in *IEEE Sensors Journal*, vol. 16, no. 17, pp. 6766-6773, Sept.1, 2016
- [57] Imagery © 2020 First Base Solutions, Maxar Technologies, Sanborn, U.S. Geological Survey, USDA Farm Service Agency.
- [58] Y. Wang, D. Vatanparvar, A. Chernyshoff and A. M. Shkel, "Analytical Closed-Form Estimation of Position Error on ZUPT-Augmented Pedestrian Inertial Navigation," in *IEEE Sensors Letters*, vol. 2, no. 4, pp. 1-4, Dec. 2018.

## APPENDICES

This thesis includes one original paper, and the paper has been accepted by IEEE Sensors Journal and published online as pre-print for early access. Therefore, the copyright release from the IEEE paper is listed below:



**IEEE**  
Requesting permission to reuse content from an IEEE publication

**Pseudo-zero velocity re-detection double threshold zero-velocity update (ZUPT) for inertial sensor-based pedestrian navigation**

Author: Tianyi Zhao  
Publication: IEEE Sensors Journal  
Publisher: IEEE  
Date: Dec 31, 1969

Copyright © 1969, IEEE

### Thesis / Dissertation Reuse

The IEEE does not require individuals working on a thesis to obtain a formal reuse license, however, you may print out this statement to be used as a permission grant:

*Requirements to be followed when using any portion (e.g., figure, graph, table, or textual material) of an IEEE copyrighted paper in a thesis:*

- 1) In the case of textual material (e.g., using short quotes or referring to the work within these papers) users must give full credit to the original source (author, paper, publication) followed by the IEEE copyright line © 2011 IEEE.
- 2) In the case of illustrations or tabular material, we require that the copyright line © [Year of original publication] IEEE appear prominently with each reprinted figure and/or table.
- 3) If a substantial portion of the original paper is to be used, and if you are not the senior author, also obtain the senior author's approval.

*Requirements to be followed when using an entire IEEE copyrighted paper in a thesis:*

- 1) The following IEEE copyright/ credit notice should be placed prominently in the references: © [year of original publication] IEEE. Reprinted, with permission, from [author names, paper title, IEEE publication title, and month/year of publication]
- 2) Only the accepted version of an IEEE copyrighted paper can be used when posting the paper or your thesis online.
- 3) In placing the thesis on the author's university website, please display the following message in a prominent place on the website: In reference to IEEE copyrighted material which is used with permission in this thesis, the IEEE does not endorse any of [university/educational entity's name goes here]'s products or services. Internal or personal use of this material is permitted. If interested in reprinting/republishing IEEE copyrighted material for advertising or promotional purposes or for creating new collective works for resale or redistribution, please go to [http://www.ieee.org/publications\\_standards/publications/rights/rights\\_link.html](http://www.ieee.org/publications_standards/publications/rights/rights_link.html) to learn how to obtain a License from RightsLink.

If applicable, University Microfilms and/or ProQuest Library, or the Archives of Canada may supply single copies of the dissertation.

BACK CLOSE WINDOW

## VITA AUCTORIS

NAME: Tianyi Zhao

PLACE OF BIRTH: Suqian, Jiangsu, China

YEAR OF BIRTH: 1994

EDUCATION: B.A.Sc. Mechanical Engineering  
University of Windsor  
Windsor, Ontario  
2014-2018

M.A.Sc. Mechanical Engineering  
University of Windsor  
Windsor, Ontario  
2019-2021